# Lymphatics in bone arise from preexisting lymphatics

Marco Monroy[1], Anna L. McCarter[1], Devon Hominick[1], Nina Cassidy[1], Michael T. Dellinger[1,2,*]

[1]Division of Surgical Oncology, Department of Surgery and the Hamon Center for Therapeutic Oncology Research, UT Southwestern Medical Center, Dallas, TX, USA. [2]Department of Molecular Biology and the Hamon Center for Regenerative Science and Medicine, UT Southwestern Medical Center, Dallas, TX, USA.

***Corresponding Author:**
Michael T. Dellinger, Ph.D.
UT Southwestern Medical Center
Hamon Center for Therapeutic Oncology Research, NB8.218
6000 Harry Hines Blvd.
Dallas, TX 75390-8593
tel: 214-648-4907
fax: 214-648-4940
email: michael.dellinger@utsouthwestern.edu

**Keywords:** Gorham-Stout disease, generalized lymphatic anomaly, VEGF-C, PIK3CA, rapamycin

**Summary Statement:** Here we show that ectopic lymphatics in bone arise from preexisting lymphatics and that rapamycin suppresses the development of lymphatics in bone.

**ABSTRACT**

Bones do not normally have lymphatics. However, patients with generalized lymphatic anomaly (GLA) or Gorham-Stout disease (GSD) develop ectopic lymphatics in bone. Despite growing interest in the development of tissue-specific lymphatics, the cellular origin of bone lymphatic endothelial cells (bLECs) is not known and the development of bone lymphatics has not been fully characterized. Here we describe the development of bone lymphatics in mouse models of GLA and GSD. Through lineage tracing experiments, we show that bLECs arise from preexisting Prox1-positive LECs. We show that bone lymphatics develop in a stepwise manner where regional lymphatics grow, breach the periosteum, and then invade bone. We also show that the development of bone lymphatics is impaired in mice that lack osteoclasts. Lastly, we show that rapamycin can suppress the growth of bone lymphatics in our models of GLA and GSD. In summary, we show that bLECs can arise from preexisting LECs and that rapamycin can prevent the growth of bone lymphatics.

## INTRODUCTION

Generalized lymphatic anomaly (GLA) and Gorham-Stout disease (GSD) are related sporadic diseases of the lymphatic system (Dellinger et al., 2014; Lala et al., 2013). Patients with GLA or GSD develop malformed lymphatics in their soft tissues and ectopic lymphatics in bone (Dellinger et al., 2014; Lala et al., 2013). The presence of lymphatics in bone is associated with bone loss, which can cause severe deformity, paralysis, and death (Dellinger et al., 2014). GLA and GSD are often difficult to treat and usually require a multidisciplinary medical team and multiple strategies. In recent years, rapamycin has become a popular treatment for GLA and GSD and it has been reported to be effective at stabilizing or reducing signs and symptoms of disease in patients (Adams et al., 2016; Cramer et al., 2016; Hammill et al., 2011; Ricci et al., 2019; Rodriguez-Laguna et al., 2019; Triana et al., 2017). Next generation sequencing studies have been performed with GLA and GSD patient samples to identify the genetic mutations responsible for these diseases. The hope is that this information could enable a precision medicine approach for the treatment of GLA and GSD. These studies have revealed that somatic activating mutations in *PIK3CA* can cause GLA (Rodriguez-Laguna et al., 2019). *PIK3CA* encodes for p110$\alpha$ (a catalytic subunit of PI3K) and the *PIK3CA* mutations in GLA patients cause hyperactivation of the PI3K/AKT/mTOR signaling pathway. A causative mutation has not been reported for GSD.

We recently developed and characterized the first mouse models of GLA and GSD. To model GLA, we used the Cre-loxP system to express an active form of *PIK3CA* (PIK3CA$^{H1047R}$) in lymphatic endothelial cells (LECs) in mice (Rodriguez-Laguna et al., 2019). We found that *Prox1-CreER$^{T2}$;LSL-Pik3ca$^{H1047R}$* mice developed a hyperbranched network of dermal lymphatics and ectopic lymphatics in bone (Rodriguez-Laguna et al., 2019). We also found that rapamycin could prevent dermal lymphatic hyperplasia and lymphatic dysfunction in *Prox1-CreER$^{T2}$;LSL-Pik3ca$^{H1047R}$* mice (Rodriguez-Laguna et al., 2019). Additionally, we found that rapamycin could attenuate dermal lymphatic hyperplasia and partially normalize lymphatic function in *Prox1-CreER$^{T2}$;LSL-Pik3ca$^{H1047R}$* mice with established disease (Rodriguez-Laguna et al., 2019). To model GSD, we used the Osterix (Osx) promoter to overexpress the lymphatic growth factor, vascular endothelial growth factor-C (VEGF-C), in bone (Hominick et al., 2018). We found that *Osx-tTA-TetO-Cre;TetO-Vegfc* mice developed lymphatics in bone and gradually lost cortical bone (Hominick et al., 2018). Loss of cortical bone is what distinguishes GSD from GLA (Lala et al., 2013). Although substantial progress has been made in our understanding of GLA and GSD, many questions still exist regarding the development of bone lymphatics. The cellular origin of bone lymphatic endothelial cells (bLECs) is not known, the stepwise development of bone lymphatics has not been fully characterized, and the effect of rapamycin on the formation of bone lymphatics has not been explored. Here we use our animal models of GLA and GSD to fill these gaps in knowledge.

## RESULTS

### *Lineage tracing of Osx-positive cells in Osx-tTA-TetO-Cre;TetO-Vegfc mice*

Table 1 provides a brief description of the different mouse strains used in this study. *Osx-tTA-TetO-Cre* mice express the tetracycline transactivator protein and Cre recombinase in osteoblasts, osteocytes, and chondrocytes (Chen et al., 2014). To determine whether bone lymphatic endothelial cells (bLECs) originate from an Osx-positive progenitor, we performed a lineage tracing experiment with *Osx-tTA-TetO-Cre;TetO-Vegfc* mice (herein referred to as *Osx-tTA;TetO-Vegfc* mice) (**Fig. 1A,B**). We used the *mT/mG* reporter mouse for all of our lineage tracing experiments. The *mT/mG* reporter allele causes Cre-positive cells and their descendants to express green fluorescent protein (GFP). It was previously reported that cells labeled by *Lyve1-Cre* during embryonic development give rise to a subset of adult hematopoietic stem cells (HSCs) (Lee et al., 2016). HSCs are stem cells that create red blood cells, white blood cells and platelets. Although a subset of adult HSCs come from a *Lyve1-Cre*-positive progenitor, they and other hematopoietic cells in the bone marrow do not express Lyve1 (Lee et al., 2016) (**Fig. S1**). Because *Lyve1-Cre;mT/mG* mice have GFP-positive cells in bone, we used bones from these mice as a positive control for immunostaining for GFP. *mT/mG* mice do not express GFP and were used as a negative control for immunostaining for GFP. We found that femurs from *Lyve1-Cre;mT/mG* mice contained numerous GFP-positive cells, whereas femurs from *mT/mG* mice did not (**Fig. 1C**). Importantly, the podoplanin-positive lymphatics in the femurs of *Osx-tTA;TetO-Vegfc;mT/mG* mice did not express GFP (**Fig.1C).** We confirmed that lymphatics in the femurs of *Osx-tTA;TetO-Vegfc;mT/mG* mice did not express GFP by staining for Lyve1 and GFP (**Fig. S2**). These results suggest that bLECs in *Osx-tTA;TetO-Vegfc* mice do not originate from an Osx-positive progenitor. Although lymphatics in the bones of *Osx-tTA;TetO-Vegfc;mT/mG* mice did not express GFP, bone cells in these mice expressed GFP in a salt and pepper fashion (**Fig. 1C; Fig S2**). This is consistent with other reports showing that bone cells are labeled by the *Osx-tTA-TetO-Cre* allele (Chen et al., 2014; Rodda and McMahon, 2006).

### *Prox1-CreER$^{T2}$ mice do not exhibit Cre activity in bone*

We then set out to determine whether bLECs originate from preexisting Prox1-positive LECs. First, we performed a lineage tracing experiment to determine whether *Prox1-CreER$^{T2}$* mice exhibit Cre activity in bone. *Prox1-CreER$^{T2}$;mT/mG* mice were injected with tamoxifen on postnatal day (P) 21, P23, P25, and P27 and femurs were collected on P55 (**Fig. 2A,B**). Femurs from *Lyve1-Cre;mT/mG* mice and *mT/mG* mice were included as controls for immunostaining for GFP. We examined GFP expression by cells in the marrow cavity, on the surface of bone, in cortical bone and in the periosseous connective tissue (**Fig. 2C**). Numerous GFP-positive cells were present in the marrow cavity of *Lyve1-Cre;mT/mG* mice (**Fig. 2D**). However, cells on the surface of bone (osteoblasts) and in cortical bone (osteocytes) did not express GFP (**Fig. 2E,F**). *mT/mG* mice and *Prox1-CreER$^{T2}$;mT/mG* mice did not have GFP-positive cells in the marrow cavity, on the surface of bone,

or in cortical bone (**Fig. 2H-N**). These results show that *Prox1-CreER$^{T2}$* mice do not exhibit Cre activity in bone. However, *Prox1-CreER$^{T2}$;mT/mG* mice had numerous GFP-positive lymphatics in their periosseous connective tissue (**Fig. 2O and Fig. S3**).

Next, we examined the leakiness of Cre activity in *Prox1-CreER$^{T2}$* mice. We examined GFP expression by lymphatics in ear skin samples from *Prox1-CreER$^{T2}$;mT/mG* mice that received tamoxifen (P21, P23, P25, and P27) and *Prox1-CreER$^{T2}$;mT/mG* mice that did not receive tamoxifen. Ear skin samples from *Lyve1-Cre;mT/mG* mice and *mT/mG* mice were included as controls for immunostaining for GFP. GFP-positive lymphatics were present in ear skin samples from *Lyve1-Cre;mT/mG* mice and *Prox1-CreER$^{T2}$;mT/mG* mice that received tamoxifen (**Fig. S4**). GFP was not present in ear skin samples from *mT/mG* mice or *Prox1-CreER$^{T2}$;mT/mG* mice that did not receive tamoxifen (**Fig. S4**). These results show that *Prox1-CreER$^{T2}$* mice do not exhibit Cre activity in the absence of tamoxifen and that our tamoxifen administration scheme effectively induces Cre-mediated recombination in LECs.

We then performed a pulse-chase experiment to determine how long it takes for the effect of tamoxifen on CreER$^{T2}$ localization to wear off in *Prox1-CreER$^{T2}$* mice. *Prox1-CreER$^{T2}$* mice were injected with tamoxifen on 21, P23, P25, and P27 and tissues were collected on P28, P41, and P55 (**Fig. 3A**). We assessed CreER$^{T2}$ localization by immunostaining with an antibody that detects the ER portion of the CreER$^{T2}$ protein. We were unable to assess the effect of tamoxifen on CreER$^{T2}$ localization in bone because *Prox1-CreER$^{T2}$* mice do not exhibit Cre activity in bone. We decided to analyze livers from *Prox-1CreER$^{T2}$* mice because Prox1 is expressed by hepatocytes and because the size and shape of hepatocytes would allow us to reliably distinguish between cytoplasmic and nuclear localization of the CreER$^{T2}$ protein. We found that CreER$^{T2}$ was localized to the nucleus on P28 but not on P41 or P55 (Fig. 3B-F). These results suggest that the effects of tamoxifen on CreER$^{T2}$ localization wear off sometime between P28 and P41. However, the kinetics of tamoxifen distribution and retention may be different in different tissues.

***Lineage tracing of Prox1-positive cells in Osx-tTA;TetO-Vegfc mice***

After we characterized Cre activity in *Prox1-CreER$^{T2}$* mice, we performed a lineage tracing experiment to determine whether bLECs arise from preexisting LECs. First, we performed several pilot studies to determine the conditions that would cause *Osx-tTA;TetO-Vegfc* mice to develop lymphatics in bone after P41 (the end of the tamoxifen washout period). We found that *Osx-tTA;TetO-Vegfc* mice developed lymphatics in bone after P41 if we gave them doxycycline water (0.2 mg/ml) from embryonic day 0.5 to P21.

Next, we gave *Osx-tTA;TetO-Vegfc;Prox1-CreER$^{T2}$;mT/mG* mice doxycycline water (0.2 mg/ml) from embryonic day 0.5 to P21 and then injected them with tamoxifen on P21, P23, P25, and P27 (**Fig. 4A,B**). We collected bones on P45 and P65 and stained them with antibodies against GFP and Lyve1. Bones collected on P45 contained numerous GFP-positive-Lyve1-negative bone cells (**Fig. 4C**). We previously showed that bone cells are labeled by *Osx-tTA-TetO-Cre*, not *Prox1-CreER$^{T2}$* (**Fig. S2, Fig. 2**). Bones collected on P45 did not have lymphatics (0 ± 0, n = 4 mice; **Figure 4C,D**). In contrast, bones collected on P65 contained Lyve1-positive lymphatics (**Fig. 4C,D**). Approximately 85% of the lymphatics expressed GFP (85.98 ± 3.227, n = 4 mice). Importantly, these lymphatics developed after the tamoxifen washout period (P28-P41).

***Stepwise development of bone lymphatics***

Next, we set out to characterize the stepwise development of bone lymphatics. We previously analyzed the development of bone lymphatics in femurs from *Osx-tTA;TetO-Vegfc* mice (Hominick et al., 2018). We reported that we could detect lymphatics in cortical bone before we could detect them in the marrow cavity (Hominick et al., 2018). It is standard practice to strip femurs free of connective tissue before fixing and decalcifying them. Because we did that in our previous study, we were not able to characterize the initial stages of development of bone lymphatics. To fill this gap in knowledge, we analyzed tissue sections where we kept the periosseous muscle tissue and periosteum intact. The periosteum is the layer of tissue that covers the outside surface of bones. We collected ribs from *TetO-Vegfc* and *Osx-tTA;TetO-Vegfc* mice on P20, P24, P28 and P32 and stained tissue cross sections with an antibody against Lyve1 (**Fig. 5A**). We then surveyed the periosseous muscle, cortical bone, and marrow cavity for lymphatics (**Fig. 5B**). Lymphatics in *TetO-Vegfc* mice were restricted to the intercostal muscle tissue and they never traversed the periosteum (**Fig. 5C-H, Table 2**). In contrast, regional lymphatics in *Osx-tTA;TetO-Vegfc* mice grew, breached the periosteum, separated the periosteum from bone, and then gradually invaded bone (**Fig. 5C-H, Table 2**).

***Osteoclasts are associated with lymphatics invading bone and the development of bone lymphatics is impaired in osteoclast-deficient mice***

Next, we characterized the invasion of bone by lymphatics. Osteoclasts are large multinucleated cells that degrade bone. Although we previously reported that *Osx-tTA;TetO-Vegfc* mice have more osteoclasts than control mice, we did not examine the relationship between osteoclasts and lymphatics in bone (Hominick et al., 2018). To determine whether osteoclasts were associated with lymphatics invading bone, we stained serial sections of bone from *Osx-tTA;TetO-Vegfc* mice for TRAP activity (marker of osteoclasts) and Lyve1. We found that osteoclasts were closely associated with invading lymphatics (**Fig. S5**).

Colony-stimulating factor 1 (Csf1) is a secreted protein that is required for the development of osteoclasts (Dai et al., 2002). To determine whether osteoclasts are required for the development of bone lymphatics, we used a genetic approach to suppress osteoclast development in *Osx-tTA;TetO-Vegfc* mice. We found that *Osx-tTA;TetO-Vegfc;Csf1*$^{mut/mut}$ mice had denser bones and significantly fewer osteoclasts than *Osx-tTA;TetO-Vegfc;Csf1*$^{wt/mut}$ mice (**Fig. 6A-F**). The density of lymphatics in the intercostal muscle tissue was not significantly different between *Osx-tTA;TetO-Vegfc;Csf1*$^{mut/mut}$ and *Osx-tTA;TetO-Vegfc;Csf1*$^{wt/mut}$ mice (**Fig. 6G,H**). This result shows that periosseous lymphangiogenesis occurs in *Osx-tTA;TetO-Vegfc;Csf1*$^{mut/mut}$ and *Osx-tTA;TetO-Vegfc;Csf1*$^{wt/mut}$ mice. In contrast to *Osx-tTA;TetO-Vegfc;Csf1*$^{wt/mut}$ mice, the cortical bone and bone marrow in *Osx-tTA;TetO-Vegfc;Csf1*$^{mut/mut}$ mice was almost completely devoid of lymphatics (**Fig. 6G,I,J)**.

***Lineage tracing of Prox1-positive cells in Prox1-CreER*$^{T2}$*;LSL-Pik3ca*$^{H1047R}$ *mice***

We previously showed that *Prox1-CreER*$^{T2}$*;LSL-Pik3ca*$^{H1047R}$ mice develop ectopic lymphatics in bone (Rodriguez-Laguna et al., 2019). Because we did not include a lineage reporter in our previous animal study (Rodriguez-Laguna et al., 2019), the origin of bLECs in *Prox1-CreER*$^{T2}$*;LSL-Pik3ca*$^{H1047R}$ mice was unclear. Therefore, we performed a lineage tracing study with *Prox1-CreER*$^{T2}$*;LSL-Pik3ca*$^{H1047R}$ mice to determine whether bLECs in these mice come from preexisting LECs. The tamoxifen injection schedule used for *Prox1-CreER*$^{T2}$*;LSL-Pik3ca*$^{H1047R}$ mice is different than the schedule used for *Osx-tTA;TetO-Vegfc;Prox1-CreER*$^{T2}$*;mT/mG* mice. Therefore, we performed another pulse-chase experiment to determine how long it takes for the effect of tamoxifen on CreER$^{T2}$ localization to wear off in *Prox1-CreER*$^{T2}$ mice. *Prox1-CreER*$^{T2}$ mice were injected with tamoxifen on P31, P33, P35, P39 and P42 and livers were collected on either P43 or P70 (**Fig. 7A**). Like before, we assessed the localization of CreER$^{T2}$ by immunostaining for ER. CreER$^{T2}$ was localized to the nucleus on P43 but not on P70 (**Fig. 7B-E**). These results suggest that the effects of tamoxifen on CreER$^{T2}$ localization wear off sometime between P43 and P70.

Next, we performed a lineage-tracing experiment with *Prox1-CreER*$^{T2}$*;LSL-Pik3ca*$^{H1047R}$*;mT/mG* mice to determine whether bLECs originate from preexisting LECs. *Prox1-CreER*$^{T2}$*;LSL-Pik3ca*$^{H1047R}$*;mT/mG* mice were injected with tamoxifen on P31, P33, P35, P39 and P42 to label LECs and femurs were collected from mice on either P43, P70 or P98 (**Fig. 7F,G**). Femurs collected on P43 and P70 did not contain lymphatics (**Fig. 7H,I**). However, femurs collected on P98 contained lymphatics and approximately 65% of the lymphatics expressed GFP (66.7 ± 33.3, n = 3) (**Fig. 7H,I**). Importantly, these lymphatics developed after the tamoxifen washout period (P43-P70).

***Rapamycin suppresses the development of bone lymphatics in Osx-tTA;TetO-Vegfc mice***

Rapamycin is an FDA-approved mTOR inhibitor that is used to treat GSD and GLA. To determine whether rapamycin could suppress the development of bone lymphatics, we treated *Osx-tTA;TetO-Vegfc* mice with rapamycin (**Fig. 8A**). We started to treat *Osx-tTA;TetO-Vegfc* mice with vehicle or rapamycin when they were 21 days old. We previously showed that *Osx-tTA;TetO-Vegfc* mice do not have lymphatics in bone when they are 21 days old (Hominick et al., 2018). We collected femurs from vehicle and rapamycin-treated mice when they were 35 days old. We found that rapamycin-treated mice had significantly fewer bone lymphatics than vehicle-treated mice (**Fig. 8B-D**). Additionally, cortical bone porosity was lower in rapamycin-treated mice than vehicle-treated mice (**Fig. 8E-G**). These results show that rapamycin can suppress the development of bone lymphatics and bone loss in *Osx-tTA;TetO-Vegfc* mice.

***Rapamycin suppresses the growth of PIK3CA-mutant LECs and the development of bone lymphatics in Prox1-CreER$^{T2}$;LSL-Pik3ca$^{H1047R}$ mice***

We then set out to characterize the effect of rapamycin on PIK3CA-mutant LECs. We obtained LECs from a patient who was reported to have a somatic activating mutation in *PIK3CA* (PIK3CA$^{H1047L}$-LECs) and a germline mutation in *PIK3R3* (Boscolo et al., 2015). We confirmed the identity of the cells by immunostaining for PROX1 and the mutation status of the cells by Sanger sequencing (**Fig. 9A-F**). We found that PIK3CA$^{H1047L}$-LECs formed irregular vessels in *in vitro* lymphangiogenesis assays (**Fig. 9G-J**). We also found that PI3K/AKT/mTORC1 signaling was greater in PIK3CA$^{H1047L}$-LECs than WT-LECs and that rapamycin could suppress mTORC1 signaling and the growth of PIK3CA$^{H1047L}$-LECs and WT-LECs (**Fig. 9K-M**). These results are consistent with other reports that rapamycin suppresses the growth of *PIK3CA*-mutant LECs (Blesinger et al., 2018; Boscolo et al., 2015; Osborn et al., 2015).

We previously showed that rapamycin could prevent dermal lymphatic hyperplasia in *Prox1-CreER$^{T2}$;LSL-Pik3ca$^{H1047R}$* mice (Rodriguez-Laguna et al., 2019). We did not characterize the effect of rapamycin on the development of bone lymphatics in our previous study (Rodriguez-Laguna et al., 2019). Therefore, we set out to determine whether rapamycin could suppress the development of bone lymphatics in *Prox1-CreER$^{T2}$;LSL-Pik3ca$^{H1047R}$* mice. Mice were injected with tamoxifen on P31, P33, P35, P39, and P42. We started to treat mice with vehicle or rapamycin on P70 (**Fig. 10A**). Our results in Figure 7 show that *Prox1-CreER$^{T2}$;LSL-Pik3ca$^{H1047R}$* mice do not have lymphatics in bone on P70 (**Fig. 7H**). We collected femurs from mice on P91. We found that rapamycin-treated mice had significantly fewer bone lymphatics than vehicle-treated mice (**Fig. 10B-D**). Eight out of 10 vehicle-treated mice had bone lymphatics whereas 0 out of 10 rapamycin-treated mice had bone lymphatics ($P < 0.001$; Fisher's exact test). These results show that rapamycin can suppress the development of bone lymphatics in *Prox1-CreER$^{T2}$;LSL-Pik3ca$^{H1047R}$* mice. We did not examine

cortical porosity in *Prox1-CreER$^{T2}$;LSL-Pik3ca$^{H1047R}$* mice because they develop a pleural effusion and die before they have significant bone involvement (Rodriguez-Laguna et al., 2019).

## DISCUSSION

In 1955, Gorham and Stout reported that patients with massive osteolysis can have ectopic lymphatics in bone (Gorham and Stout, 1955). Since that groundbreaking observation, investigators have been interested in the development of bone lymphatics and in identifying drugs that could inhibit the growth of lymphatics in bone. In the present study, we show that bLECs can arise from preexisting LECs and that rapamycin can suppress the development of bone lymphatics.

LECs can arise from multiple different cell types. Lineage tracing studies in mice have shown that LECs can arise from preexisting LECs (Srinivasan et al., 2007), hemogenic endothelium (Stanczuk et al., 2015), blood endothelium (Martinez-Corral et al., 2015; Pichol-Thievend et al., 2018; Srinivasan et al., 2007), and from an unknown cellular source (Martinez-Corral et al., 2015). Bone marrow transplantation studies have shown that LECs can also develop from the hematopoietic lineage (Jiang et al., 2008). Additionally, tissue culture experiments have shown that macrophages and mesenchymal stem cells can express markers of lymphatic endothelium under certain culture conditions (Conrad et al., 2009; Hall et al., 2012). The cellular origin of bLECs was not previously known. We found that most of the bLECs in *Osx-tTA;TetO-Vegfc* and *Prox1-CreER$^{T2}$;LSL-Pik3ca$^{H1047R}$* mice came from preexisting Prox1-positive cells. However, not all of the bLECs in our mouse models expressed the lineage reporter. This could be due to an incomplete labeling of LECs in our animal models. Alternatively, a small fraction of bLECs could come from a different cellular source. As more lymphatic endothelial progenitors are identified, additional lineage tracing studies could be performed to determine whether other cell types give rise to bLECs.

We found that *Osx-tTA;TetO-Vegfc* mice that were exposed to doxycycline from E0.5 to P21 developed lymphatics in bone slower than mice that were exposed to doxycycline from E0.5 to E18.5. Tetracyclines, such as doxycycline, incorporate into mineralizing bone (Pautke et al., 2010). Because mice in the lineage tracing study were exposed to doxycycline for a longer period of time, they could have accumulated more doxycycline in bone and required more time for the doxycycline to washout. This could impact the expression of VEGF-C because we use a Tet-Off system to control the expression of VEGF-C by bone cells. Another possible explanation is that bones in old mice might be more resistant to the development of bone lymphatics than bones in young mice.

We previously analyzed the development of bone lymphatics in femurs from *Osx-tTA;TetO-Vegfc* mice (Hominick et al., 2018). However, we were not able to examine the initial stages of bone lymphatic development because we peeled away the periosseous muscle tissue from our samples.

In the present study, we analyzed samples where we kept the periosseous tissue intact. This allowed us to gain further insight into the development of bone lymphatics. We found that lymphatics in control mice were restricted to the periosseous muscle tissue and they never crossed the periosteum. This raises the possibility that the periosteum protects bones from lymphatics. Additionally, the periosteum may express factors that prevent lymphatics from invading bone. Future *in vitro* and *in vivo* experiments could reveal whether the periosteum shields bones from lymphatics and inhibits lymphangiogenesis. In contrast to control mice, mutant mice had lymphatics that grew, breached the periosteum, and then separated the periosteum from the underlying bone. The periosteum contains progenitor cells that differentiate into osteoblasts, which are cells that synthesize new bone (Dwek, 2010). Therefore, lymphatics in mutant mice might affect bone regeneration and repair by coming between the periosteum and bone. If this occurs in patients, it could contribute to the bone regeneration/repair defects observed in GLA and GSD.

Lymphatics need to pass through cortical bone before they colonize the marrow cavity. We previously showed that LECs cannot directly degrade a matrix that mimics bone (Hominick et al., 2018). Therefore, a different cell type must clear the way for LECs. Osteoclasts are large multinucleated cells that resorb bone. We previously reported that *Osx-tTA;TetO-Vegfc* mice have more osteoclasts than control mice (Hominick et al., 2018). In the present study we characterized the relationship between osteoclasts and lymphatics. We found that osteoclasts were closely associated with lymphatics invading bone. This raises the possibility that osteoclasts clear a path through bone for LECs. The close association between osteoclasts and lymphatics also raises the possibility that these two cell types communicate with one another. Indeed, LECs have been reported to secrete M-CSF, a factor that promotes osteoclast development, and conditioned media from LECs has been shown to promote the formation of osteoclasts in a M-CSF-dependent manner (Wang et al., 2017). Conversely, osteoclasts have been reported to express VEGF-C (Zhang et al., 2008). The potential crosstalk between LECs and osteoclasts may serve an important role in the development of bone lymphatics. In the future, M-CSF could be conditionally deleted in LECs to determine whether its production by LECs promotes osteoclast formation *in vivo* and the invasion of bone by lymphatics.

We previously reported that zoledronic acid (an osteoclast inhibitor) attenuated bone loss, but not the development of bone lymphatics, in *Osx-tTA;TetO-Vegfc* mice (Hominick et al., 2018). However, here we report that the invasion of bone by lymphatics is impaired in *Osx-tTA;TetO-Vegfc;Csf1*$^{mut/mut}$ mice. One potential reason for this discrepancy is that the different approaches we used to inhibit osteoclasts differ in their ability to block osteoclast development and activity. Although zoledronic acid-treated mice had fewer osteoclasts than vehicle-treated mice (Hominick et al., 2018), they still had osteoclasts. In contrast, *Osx-tTA;TetO-Vegfc;Csf1*$^{mut/mut}$ mice completely lacked osteoclasts. It

is possible that the remaining osteoclasts in zoledronic acid-treated mice were sufficient to facilitate the development of bone lymphatics. It is also possible that the structural changes to bone in *Osx-tTA;TetO-Vegfc;Csf1*$^{mut/mut}$ mice make the bone impenetrable to lymphatics or that the loss of other Csf1-dependent cells impairs the development of lymphatics in bone in *Osx-tTA;TetO-Vegfc;Csf1*$^{mut/mut}$ mice. Presently, we are not able to distinguish between these possibilities.

In recent years, enthusiasm has grown for the FDA-approved drug rapamycin, because it has been found to have remarkable effects on the lymphatic system. Preclinical studies with mice that overexpress VEGF-C in the lung (*CCSP-rtTA;TetO-Vegfc* mice) revealed that rapamycin can suppress VEGF-C-induced lymphangiogenesis and partially reverse VEGF-C-driven lymphangiectasia and we have shown that rapamycin can suppress lymphangiogenesis in the skin of *Prox1-CreER*$^{T2}$*;LSL-Pik3ca*$^{H1047R}$ mice (Baluk et al., 2017; Rodriguez-Laguna et al., 2019). In the clinic, rapamycin has been found to be an effective treatment for lymphatic anomalies such as GLA and GSD (Adams et al., 2016; Cramer et al., 2016; Hammill et al., 2011; Ricci et al., 2019; Rodriguez-Laguna et al., 2019; Triana et al., 2017). A recent study examined the effect of rapamycin on disease response in 13 patients with GLA and 5 patients with GSD (Ricci et al., 2019). Bone disease did not progress in any of the patients while they were on rapamycin (Ricci et al., 2019). Amazingly, it was reported that 1 patient with GLA had a complete resolution of their bone disease (Ricci et al., 2019). The evaluation of bones in patients treated with rapamycin has been limited to imaging (MRI, CT and X-ray). This has made it difficult to determine the effect of rapamycin on bone lymphatics in GLA and GSD patients. By examining the histology of bones, we were able to show for the first time that rapamycin can inhibit the development of bone lymphatics. We also show that rapamycin can attenuate bone loss in *Osx-tTA;TetO-Vegfc* mice. One outstanding question is whether rapamycin can induce the regression of lymphatics in bone. Unfortunately, a majority of our *Osx-tTA;TetO-Vegfc* and *Prox1-CreER*$^{T2}$*;LSL-Pik3ca*$^{H1047R}$ mice develop a pleural effusion and die shortly after they develop lymphatics in bone. This makes reversal studies with our models extremely challenging. Although we do not show that rapamycin can cause lymphatics in bone to regress, we believe that our preclinical findings provide further support for the testing of rapamycin in GLA and GSD patients.

Taken together, our results shed light on the development of bone lymphatics, a process that has puzzled investigators since Gorham and Stout published their landmark paper over 60 years ago. We also provide preclinical data that shows that rapamycin, an emerging treatment for patients, can suppress the development of lymphatics in bone.

## MATERIALS AND METHODS

### *Mice and genotyping*

The animal experiments described in this manuscript were carried out in accordance with an animal protocol approved by the Institutional Animal Care and Use Committee of UT Southwestern Medical Center.

Mice were maintained in ventilated microisolator cages and were fed a standard diet *ad libitum*. Mice were provided igloos and nestlets as enrichment items. Both males and females were used in experiments. Littermates were used as controls for experiments. *TetO-Vegfc* (Lohela et al., 2008), *mT/mG* (Muzumdar et al., 2007), *Osx-tTA* (Rodda and McMahon, 2006), *Lyve1-Cre* (Pham et al., 2010), *LSL-Pik3ca*$^{H1047R}$ (Adams et al., 2011) and *Prox1-CreER*$^{T2}$ (Srinivasan et al., 2007) mice were genotyped as previously described (Dellinger et al., 2013; Hominick et al., 2018; Rodriguez-Laguna et al., 2019). *Csf1* mutant mice (Yoshida et al., 1990) were purchased from the Jackson Laboratory (Stock number: 000231) and were genotyped with the following primers: 5'-GCCTAGGGTGTGATCGTCTC-3'; and 5'- TAAGGTTCAGGCTCGGTGAG-3'. PCR products were then sequenced to look for the presence of the causative genetic mutation (mutation = T insertion).

### *Doxycycline administration*

We used the Tet-Off system to control the expression of VEGF-C by osterix-positive bone cells. Mice on normal drinking water express VEGF-C in bone whereas mice on doxycycline water do not express VEGF-C in bone. Mice received water containing sucrose (5% w/v) and doxycycline (0.2 mg/ml or 1 mg/ml; Sigma-Aldrich, D9891) as indicated in the figure legends. Doxycycline water was replaced 3 times a week.

### *Preparation of tamoxifen and rapamycin*

Tamoxifen (20 mg; Sigma, T5648) was dissolved in a mixture of ethanol (100 µl; Sigma, E7023) and sunflower oil (900 µl; Sigma, W530285). Mice received 100 µl of tamoxifen via an intraperitoneal injection. Rapamycin (Enzo, BML-A275-0025) was dissolved in ethanol to make a stock solution (50 mg/ml). The stock solution was then diluted to 1 mg/ml in a saline solution that contained polyethylene glycol (5% w/v; Sigma, 88440) and Tween 80 (5% w/v; Sigma, P4780). Mice received 100 µg of rapamycin 5 times a week via an intraperitoneal injection.

### *Antibodies*

The following primary antibodies were used for western blot analysis, immunohistochemistry, or immunofluorescence staining: goat anti-Lyve1 (R&D Systems, #AF2125, dilution 1:250), chicken anti-GFP (abcam, #ab13970, dilution 1:4000), hamster anti-podoplanin (abcam, #ab11936, dilution 1:1000), rabbit anti-phospho-AKT T308 (Cell Signaling, #13038, dilution 1:1000), rabbit anti-phospho-AKT S473 (Cell Signaling, #4060, dilution 1:1000), rabbit anti-AKT (Cell Signaling, #4685,

dilution 1:1000), D2-40 (abcam, #ab52092, prediluted by company), rabbit anti-estrogen receptor (abcam, #ab27595, prediluted by company), rabbit anti-PROX1 (Cell Signaling, #14963, dilution 1:100), rabbit anti-phospho-S6 S240/244 (Cell Signaling, #2D68F8, dilution 1:1000), and rabbit anti-S6 (Cell Signaling, #2217, dilution 1:1000).

***Tissue fixation and decalcification***

Mice were euthanized and then perfused with PBS + heparin and then with 4% PFA. Bones were fixed overnight in 4% PFA and then decalcified for 2 weeks in 10% EDTA (pH, 7.4). Bones were then processed and embedded by the histology core at UT Southwestern Medical Center.

***Immunohistochemistry***

Slides were deparaffinized and then rehydrated. A hydrogen peroxide/methanol solution was used to block endogenous peroxidase activity and TBST + 20% Aquablock was used to block nonspecific binding of antibodies. Slides were incubated overnight with primary antibodies diluted in TBST + 5% BSA. Slides were washed with TBST then incubated for 1 hour with secondary antibodies diluted in TBST + 5% BSA. Antibody binding was detected with an ImmPACT DAB Peroxidase Substrate Kit (Vector, SK-4105), which creates a brown color. Slides were then dipped in hematoxylin (purple color), dehydrated, and coverslips were mounted with CytoSeal (Thermoscientific, 8312-4). A similar protocol was used to stain liver sections, except antigen retrieval was performed with a 1X Tris-EDTA + 10% glycerol solution and a modified secondary antibody (Vector, MP-7451) was used to detect the anti-ER primary antibody. We did not dip slides of liver in hematoxylin so we could visualize nuclear ER staining.

***Quantification of bone lymphatics***

*Lymphatic Vessel Index*.

Images were captured with a 40X objective and were analyzed in Image J. A 20-line by 26-line multipurpose test grid, with line length 9 μm, spacing 9 μm, total points 520, and total test area 180 μm x 235 μm, was overlaid on images with tissue dimensions of 180 μm x 235 μm. The total test area was 42,300 $\mu m^2$. We counted the number of times the gridlines intersected on lymphatics and in lymphatic lumens in the test area. We refer to this value as “Lymphatic Vessel Index”.

*Lymphatics per femur section*.

To determine the number of lymphatics per femur section, we scanned an entire 5 μm-thick longitudinal section of femur and counted the number of bone lymphatics in the section.

***Assessment of GFP expression by lymphatics***

Serial sections of bone were stained with antibodies against GFP and either Lyve1 or podoplanin. We captured images of the slides and then counted the number of GFP-positive and GFP-negative lymphatics.

***Tartrate-resistant acid phosphatase (TRAP) staining and cortical porosity measurements***

TRAP staining and cortical porosity measurements were performed as previously described (Hominick et al., 2018).

***Cell culture***

Primary adult human dermal LECs were purchased from LONZA (CC-2810). Cells were cultured on rat-tail collagen 1 (50 µg/ml) or fibronectin-coated plasticware in EGM-2MV media (LONZA CC-3125). PIK3CA$^{H1047L}$-LECs were obtained from Dr. Joyce Bischoff. These cells were isolated from a lymphatic malformation from a patient (Boscolo et al., 2015). Cells were found to be mycoplasma-negative with a mycoplasma PCR detection kit (iNtRON, #25235).

***Western blot analysis***

Cells were scraped in lysis buffer (mPER [Thermo Scientific, #78501] +Protease Inhibitor [Thermo Scientific, #78425] +Phosphatase Inhibitors I and II [Sigma-Aldrich, P2850 and P5726]), spun for 10 minutes at 4°C, and then supernatants were transferred to new tubes. Protein concentration was determined by performing a BCA assay. Equal amounts of protein were separated by SDS-PAGE then transferred to PVDF membranes. Membranes were blocked for 30 minutes at room temperature with either TBST+5% BSA or TBST+5% non-fat milk, incubated overnight at 4°C with phospho-specific primary antibodies, washed with TBST, and then incubated for 1 hour at room temperature with the appropriate HRP-conjugated secondary antibodies. Bound antibodies were detected with the SuperSignal West Pico PLUS Substrate detection system (Thermo Scientific, #34577). Membranes were re-blocked then re-probed with antibodies to detect the total level of target proteins.

***In vitro lymphangiogenesis assays***

A previously published protocol for HUVECs was used for the fibrin-bead assay with LECs (Nakatsu and Hughes, 2008). For fibroblast-LEC co-culture assays, primary human lung fibroblasts (PHLFs) were seeded in chambers of a 4-well chamber slide. When the PHLFs were approximately 90% confluent, 50,000 LECs were added to the chambers. Cells were cultured for 6-7 days and media (EGM-2MV) was changed every other day. Chambers were washed with PBS and cells were fixed for 10 minutes with ice-cold methanol. Cells were washed with PBS then treated with PBS + 20% Aquablock to block nonspecific binding of the primary antibody. Slides were incubated overnight

with D2-40 (abcam, ab52092), washed with PBS, then incubated with the appropriate secondary antibody diluted in PBS. Slides were then washed with PBS and coverslips were mounted with ProLong Gold plus DAPI (Invitrogen, P36931).

### *ICC staining of LECs*

Cells were grown in the wells of a chamber slide. Old media was washed off with PBS. Cells were then fixed with ice-cold methanol for 10 minutes. Cells were then washed with PBS and blocked with PBS + 20% Aquablock for 30 minutes. Cells were incubated overnight at 4°C with primary antibodies diluted in PBS + 0.1% Tween20. Cells were washed and then incubated for 1 hour with secondary antibodies diluted in PBS. Cells were washed again and coverslips were mounted with ProLong Gold plus DAPI.

### *Cell viability assay*

LECs (5,000 cells per well) were seeded into the wells of a Falcon Optilux Black/Clear bottom 96-well plate. The media was changed the next day and DMSO or rapamycin was added to the wells. Three days later, viability was assessed with either Cell Titer Blue (Promega, G8081) or MTS reagent.

### *Statistical analysis*

Data were analyzed using GraphPad Prism statistical analysis software (Version 7.0). All results are expressed as mean ± SEM. The number of mice in each group is indicated in the figure legends (n = number of mice). For experiments with two groups, unpaired Student's *t*-tests were performed to test means for significance. For experiments with more than two groups, differences were assessed by ANOVA followed by Dunnett's multiple comparisons test. Data were considered significant at $P < 0.05$.

## AUTHOR CONTRIBUTIONS

MM, ALM, NC and DH conducted experiments. MTD designed the experiments, conducted experiments and wrote the paper. All authors reviewed and edited the manuscript.


## ACKNOWLEDGEMENTS

The authors would like to thank Joyce Bischoff for the PIK3CA$^{H1047L}$-LECs, Kari Alitalo for the *TetO-Vegfc* mouse line, Rolf Brekken for comments on the manuscript and Jack Kelly (president of the Lymphangiomatosis & Gorham's Disease Alliance) and Tiffany Ferry (president of the Lymphatic Malformation Institute) for their support. The authors would also like to thank David Primm for help in editing the manuscript.


## COMPETING INTERESTS

MTD is the Director of Research for the Lymphatic Malformation Institute. The other authors declare no competing or financial interests.


## FUNDING

This work was supported by a grant from the NIH (1R01HL144793-01) to MTD. Nina Cassidy was supported by the SURF program at UT Southwestern.

## REFERENCES


**Adams, D. M., Trenor, C. C., 3rd, Hammill, A. M., Vinks, A. A., Patel, M. N., Chaudry, G., Wentzel, M. S., Mobberley-Schuman, P. S., Campbell, L. M., Brookbank, C., et al.** (2016). Efficacy and Safety of Sirolimus in the Treatment of Complicated Vascular Anomalies. *Pediatrics* **137**, 1-10.

**Adams, J. R., Xu, K., Liu, J. C., Agamez, N. M., Loch, A. J., Wong, R. G., Wang, W., Wright, K. L., Lane, T. F., Zacksenhaus, E., et al.** (2011). Cooperation between Pik3ca and p53 mutations in mouse mammary tumor formation. *Cancer research* **71**, 2706-2717.

**Baluk, P., Yao, L. C., Flores, J. C., Choi, D., Hong, Y. K. and McDonald, D. M.** (2017). Rapamycin reversal of VEGF-C-driven lymphatic anomalies in the respiratory tract. *JCI Insight* **2**.

**Blesinger, H., Kaulfuss, S., Aung, T., Schwoch, S., Prantl, L., Rossler, J., Wilting, J. and Becker, J.** (2018). PIK3CA mutations are specifically localized to lymphatic endothelial cells of lymphatic malformations. *PloS one* **13**, e0200343.

**Boscolo, E., Coma, S., Luks, V. L., Greene, A. K., Klagsbrun, M., Warman, M. L. and Bischoff, J.** (2015). AKT hyper-phosphorylation associated with PI3K mutations in lymphatic endothelial cells from a patient with lymphatic malformation. *Angiogenesis* **18**, 151-162.

**Chen, J., Shi, Y., Regan, J., Karuppaiah, K., Ornitz, D. M. and Long, F.** (2014). Osx-Cre targets multiple cell types besides osteoblast lineage in postnatal mice. *PloS one* **9**, e85161.

**Conrad, C., Niess, H., Huss, R., Huber, S., von Luettichau, I., Nelson, P. J., Ott, H. C., Jauch, K. W. and Bruns, C. J.** (2009). Multipotent mesenchymal stem cells acquire a lymphendothelial phenotype and enhance lymphatic regeneration in vivo. *Circulation* **119**, 281-289.

**Cramer, S. L., Wei, S., Merrow, A. C. and Pressey, J. G.** (2016). Gorham-Stout Disease Successfully Treated With Sirolimus and Zoledronic Acid Therapy. *Journal of pediatric hematology/oncology* **38**, e129-132.

**Dai, X. M., Ryan, G. R., Hapel, A. J., Dominguez, M. G., Russell, R. G., Kapp, S., Sylvestre, V. and Stanley, E. R.** (2002). Targeted disruption of the mouse colony-stimulating factor 1 receptor gene results in osteopetrosis, mononuclear phagocyte deficiency, increased primitive progenitor cell frequencies, and reproductive defects. *Blood* **99**, 111-120.

**Dellinger, M. T., Garg, N. and Olsen, B. R.** (2014). Viewpoints on vessels and vanishing bones in Gorham-Stout disease. *Bone* **63**, 47-52.

**Dellinger, M. T., Meadows, S. M., Wynne, K., Cleaver, O. and Brekken, R. A.** (2013). Vascular endothelial growth factor receptor-2 promotes the development of the lymphatic vasculature. *PloS one* **8**, e74686.

**Dwek, J. R.** (2010). The periosteum: what is it, where is it, and what mimics it in its absence? *Skeletal radiology* **39**, 319-323.

**Gorham, L. W. and Stout, A. P.** (1955). Massive osteolysis (acute spontaneous absorption of bone, phantom bone, disappearing bone); its relation to hemangiomatosis. *The Journal of bone and joint surgery. American volume* **37-A**, 985-1004.

**Hall, K. L., Volk-Draper, L. D., Flister, M. J. and Ran, S.** (2012). New model of macrophage acquisition of the lymphatic endothelial phenotype. *PloS one* **7**, e31794.

**Hammill, A. M., Wentzel, M., Gupta, A., Nelson, S., Lucky, A., Elluru, R., Dasgupta, R., Azizkhan, R. G. and Adams, D. M.** (2011). Sirolimus for the treatment of complicated vascular anomalies in children. *Pediatric blood & cancer* **57**, 1018-1024.

**Hominick, D., Silva, A., Khurana, N., Liu, Y., Dechow, P. C., Feng, J. Q., Pytowski, B., Rutkowski, J. M., Alitalo, K. and Dellinger, M. T.** (2018). VEGF-C promotes the development of lymphatics in bone and bone loss. *Elife* **7**.

**Jiang, S., Bailey, A. S., Goldman, D. C., Swain, J. R., Wong, M. H., Streeter, P. R. and Fleming, W. H.** (2008). Hematopoietic stem cells contribute to lymphatic endothelium. *PloS one* **3**, e3812.

**Lala, S., Mulliken, J. B., Alomari, A. I., Fishman, S. J., Kozakewich, H. P. and Chaudry, G.** (2013). Gorham-Stout disease and generalized lymphatic anomaly-clinical, radiologic, and histologic differentiation. *Skeletal radiology* **42**, 917-924.

**Lee, L. K., Ghorbanian, Y., Wang, W., Wang, Y., Kim, Y. J., Weissman, I. L., Inlay, M. A. and Mikkola, H. K. A.** (2016). LYVE1 Marks the Divergence of Yolk Sac Definitive Hemogenic Endothelium from the Primitive Erythroid Lineage. *Cell reports* **17**, 2286-2298.

**Lohela, M., Helotera, H., Haiko, P., Dumont, D. J. and Alitalo, K.** (2008). Transgenic induction of vascular endothelial growth factor-C is strongly angiogenic in mouse embryos but leads to persistent lymphatic hyperplasia in adult tissues. *The American journal of pathology* **173**, 1891-1901.

**Martinez-Corral, I., Ulvmar, M. H., Stanczuk, L., Tatin, F., Kizhatil, K., John, S. W., Alitalo, K., Ortega, S. and Makinen, T.** (2015). Nonvenous origin of dermal lymphatic vasculature. *Circulation research* **116**, 1649-1654.

**Muzumdar, M. D., Tasic, B., Miyamichi, K., Li, L. and Luo, L.** (2007). A global double-fluorescent Cre reporter mouse. *Genesis* **45**, 593-605.

**Nakatsu, M. N. and Hughes, C. C.** (2008). An optimized three-dimensional in vitro model for the analysis of angiogenesis. *Methods Enzymol* **443**, 65-82.

**Osborn, A. J., Dickie, P., Neilson, D. E., Glaser, K., Lynch, K. A., Gupta, A. and Dickie, B. H.** (2015). Activating PIK3CA alleles and lymphangiogenic phenotype of lymphatic endothelial cells isolated from lymphatic malformations. *Human molecular genetics* **24**, 926-938.

**Pautke, C., Vogt, S., Kreutzer, K., Haczek, C., Wexel, G., Kolk, A., Imhoff, A. B., Zitzelsberger, H., Milz, S. and Tischer, T.** (2010). Characterization of eight different tetracyclines: advances in fluorescence bone labeling. *J Anat* **217**, 76-82.

**Pham, T. H., Baluk, P., Xu, Y., Grigorova, I., Bankovich, A. J., Pappu, R., Coughlin, S. R., McDonald, D. M., Schwab, S. R. and Cyster, J. G.** (2010). Lymphatic endothelial cell sphingosine kinase activity is required for lymphocyte egress and lymphatic patterning. *The Journal of experimental medicine* **207**, 17-27.

**Pichol-Thievend, C., Betterman, K. L., Liu, X., Ma, W., Skoczylas, R., Lesieur, E., Bos, F. L., Schulte, D., Schulte-Merker, S., Hogan, B. M., et al.** (2018). A blood capillary plexus-derived population of progenitor cells contributes to genesis of the dermal lymphatic vasculature during embryonic development. *Development* **145**.

**Ricci, K. W., Hammill, A. M., Mobberley-Schuman, P., Nelson, S. C., Blatt, J., Bender, J. L. G., McCuaig, C. C., Synakiewicz, A., Frieden, I. J. and Adams, D. M.** (2019). Efficacy of systemic sirolimus in the treatment of generalized lymphatic anomaly and Gorham-Stout disease. *Pediatric blood & cancer* **66**, e27614.

**Rodda, S. J. and McMahon, A. P.** (2006). Distinct roles for Hedgehog and canonical Wnt signaling in specification, differentiation and maintenance of osteoblast progenitors. *Development* **133**, 3231-3244.

**Rodriguez-Laguna, L., Agra, N., Ibanez, K., Oliva-Molina, G., Gordo, G., Khurana, N., Hominick, D., Beato, M., Colmenero, I., Herranz, G., et al.** (2019). Somatic activating mutations in PIK3CA cause generalized lymphatic anomaly. *The Journal of experimental medicine* **216**, 407-418.

**Srinivasan, R. S., Dillard, M. E., Lagutin, O. V., Lin, F. J., Tsai, S., Tsai, M. J., Samokhvalov, I. M. and Oliver, G.** (2007). Lineage tracing demonstrates the venous origin of the mammalian lymphatic vasculature. *Genes & development* **21**, 2422-2432.

**Stanczuk, L., Martinez-Corral, I., Ulvmar, M. H., Zhang, Y., Lavina, B., Fruttiger, M., Adams, R. H., Saur, D., Betsholtz, C., Ortega, S., et al.** (2015). cKit Lineage Hemogenic Endothelium-Derived Cells Contribute to Mesenteric Lymphatic Vessels. *Cell reports*.

**Triana, P., Dore, M., Cerezo, V. N., Cervantes, M., Sanchez, A. V., Ferrero, M. M., Gonzalez, M. D. and Lopez-Gutierrez, J. C.** (2017). Sirolimus in the Treatment of Vascular Anomalies. *European journal of pediatric surgery : official journal of Austrian Association of Pediatric Surgery ... [et al] = Zeitschrift fur Kinderchirurgie* **27**, 86-90.

**Wang, W., Wang, H., Zhou, X., Li, X., Wen, S., Dellinger, M., Boyce, B. F. and Xing, L.** (2017). Lymphatic Endothelial Cells Produce M-CSF Causing Massive Bone Loss in Mice. *Journal of bone and mineral research : the official journal of the American Society for Bone and Mineral Research*.

**Yoshida, H., Hayashi, S., Kunisada, T., Ogawa, M., Nishikawa, S., Okamura, H., Sudo, T., Shultz, L. D. and Nishikawa, S.** (1990). The murine mutation osteopetrosis is in the coding region of the macrophage colony stimulating factor gene. *Nature* **345**, 442-444.

**Zhang, Q., Guo, R., Lu, Y., Zhao, L., Zhou, Q., Schwarz, E. M., Huang, J., Chen, D., Jin, Z. G., Boyce, B. F., et al.** (2008). VEGF-C, a lymphatic growth factor, is a RANKL target gene in osteoclasts that enhances osteoclastic bone resorption through an autocrine mechanism. *The Journal of biological chemistry* **283**, 13491-13499.

## Figures

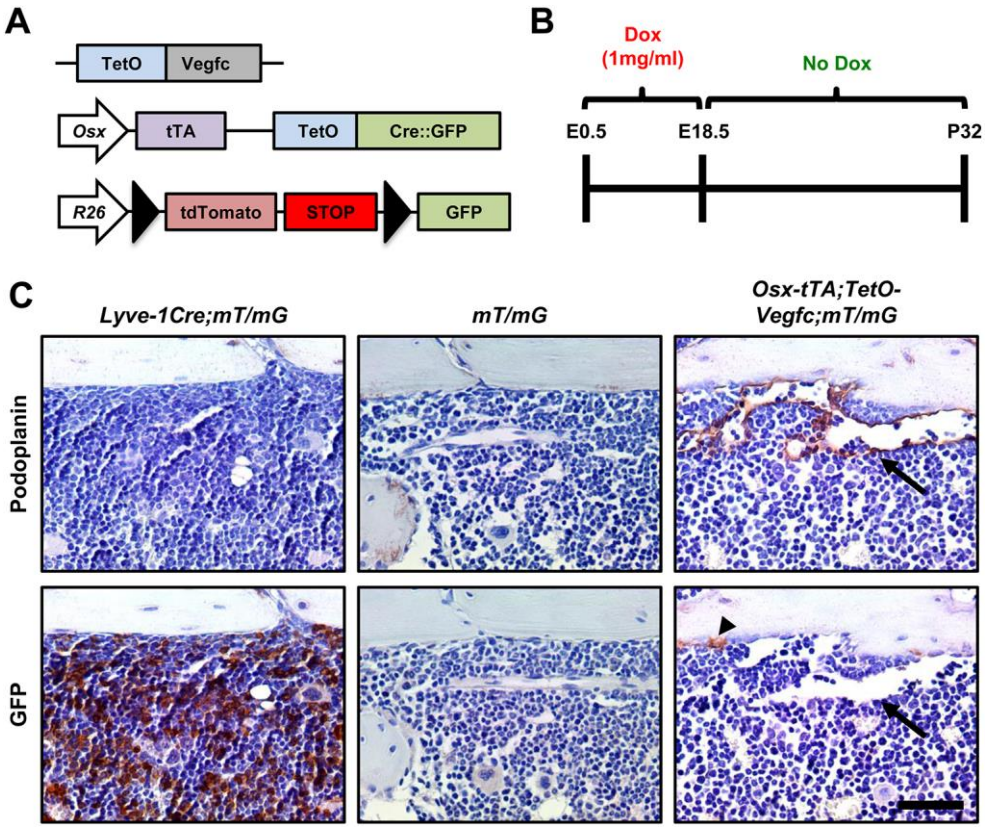


**Figure 1. Lineage tracing of Osx-positive cells in *Osx-tTA-TetO-Cre;TetO-Vegfc;mT/mG* mice.** **A.** Schematics of the *TetO-Vegfc* transgene, *Osx-tTA-TetO-Cre* transgene, and *mT/mG* reporter. **B.** Schematic showing when *Osx-tTA-TetO-Cre;TetO-Vegfc;mT/mG* mice received doxycycline water (1 mg/ml). **C.** Representative images of serial sections stained with antibodies against podoplanin and GFP. We analyzed femurs from *Lyve-1-Cre;mT/mG* mice (n = 3 mice), *mT/mG* mice (n = 3 mice), and *Osx-tTA-TetO-Cre;TetO-Vegfc;mT/mG* mice (n = 3 mice). The podoplanin-positive lymphatics in *Osx-tTA-TetO-Cre;TetO-Vegfc;mT/mG* mice did not express GFP (0/24 lymphatics; 0 ± 0, n = 3). The arrow points to a GFP-negative lymphatic in a femur from an *Osx-tTA-TetO-Cre;TetO-Vegfc;mT/mG* mouse. The arrowhead points to a GFP-positive bone cell in a femur from an *Osx-tTA-TetO-Cre;TetO-Vegfc;mT/mG* mouse. Scale bar: 50 μm.

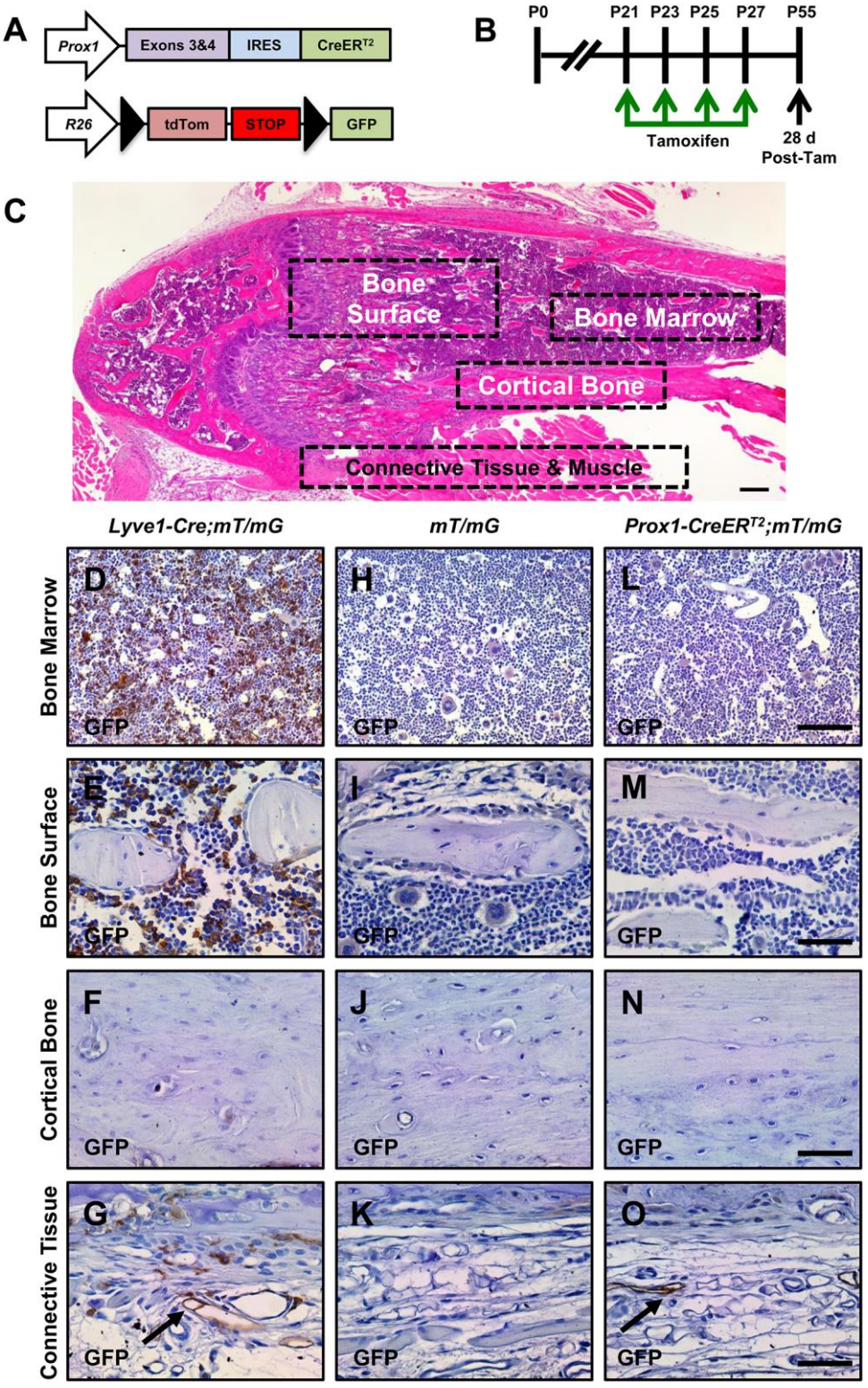


**Figure 2. *Prox1-CreER$^{T2}$* mice do not exhibit Cre activity in bone. A.** Schematics of the *Prox1-CreER$^{T2}$* construct and *mT/mG* reporter. **B.** Schematic showing when *Prox1-CreER$^{T2}$;mT/mG* mice were injected with tamoxifen (2 mg; i.p.). **C.** Low magnification image of an H&E-stained femur that shows the different areas analyzed in *Lyve-1Cre;mT/mG*, *mT/mG*, and *Prox1-CreER$^{T2}$;mT/mG*

mice. **D-O.** Representative images of femurs stained with an anti-GFP antibody. Femurs were analyzed from *Lyve-1Cre;mT/mG* mice (positive control; n = 3 mice), *mT/mG* mice (negative control; n = 3 mice) and *Prox1-CreER$^{T2}$;mT/mG* mice (n = 3 mice). GFP was not expressed by cells in the marrow cavity, cortical bone, or on the surface of bone (osteoblasts and osteoclasts) in *Prox1-CreER$^{T2}$;mT/mG* mice. The arrows in G and O point to GFP-positive lymphatics in periosseous connective tissue. Panel C scale bar: 200 μm. Panel L scale bar: 100 μm. Panels M, N, and O scale bar: 50 μm.

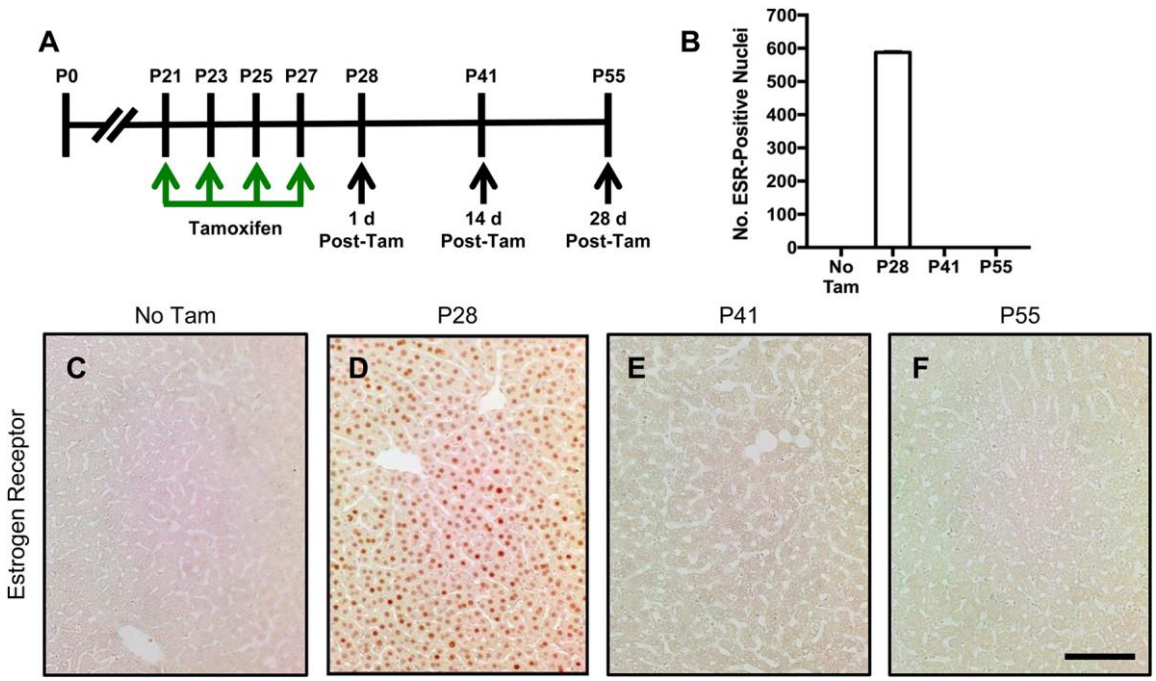


**Figure 3. Localization of Cre recombinase in *Prox1-CreER$^{T2}$* mice. A.** Schematic showing when *Prox1-CreER$^{T2}$* mice were injected with tamoxifen (2 mg; i.p.). **B.** Graph showing the number of estrogen receptor-positive nuclei in livers from *Prox1-CreER$^{T2}$* mice that did not receive tamoxifen (0 ± 0, n = 3) and from *Prox1-CreER$^{T2}$* mice 1 day (588 ± 3.22, n = 3), 14 days (0 ± 0, n = 3), and 28 days (0 ± 0, n = 3) after they received their last pulse of tamoxifen. **C-F.** Representative images of livers stained with an anti-estrogen receptor antibody. CreER$^{T2}$ moved out of the nucleus sometime between P28 and P41. Data are presented as mean ± SEM. Scale bar: 100 μm

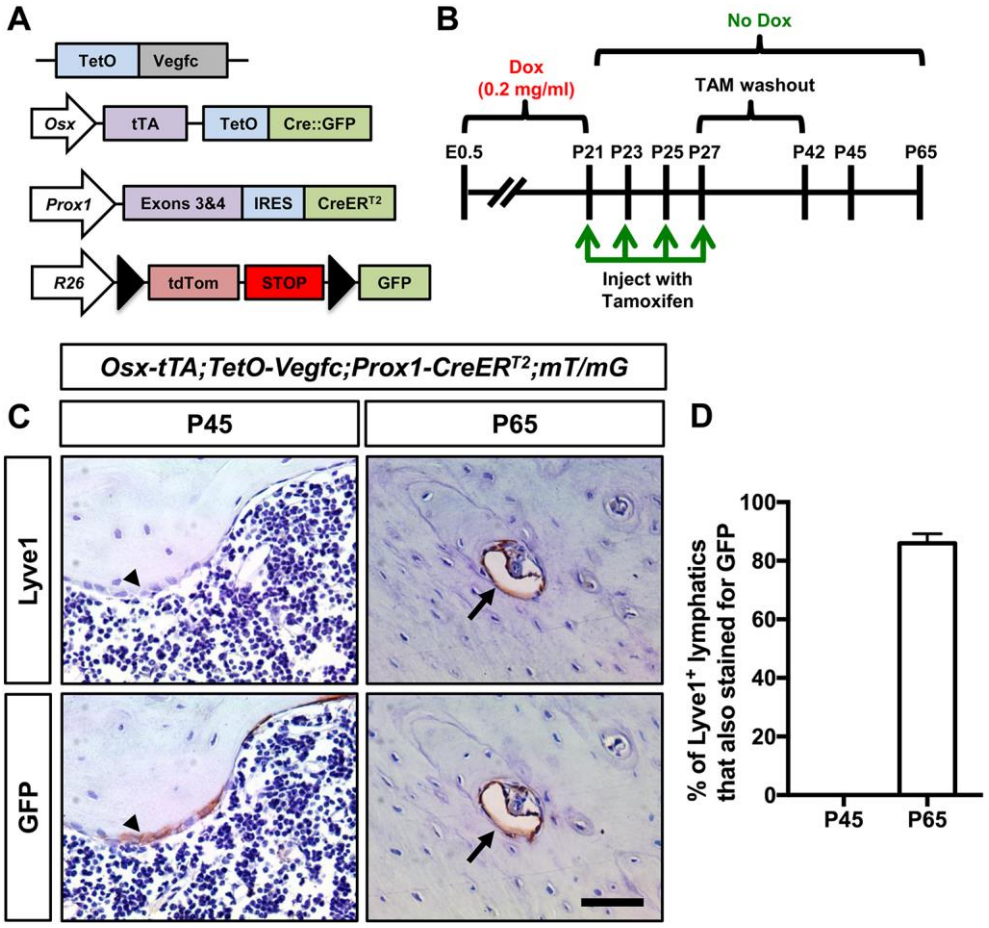


**Figure 4. Lineage tracing of Prox1-positive cells in *Osx-tTA;TetO-Vegfc* mice. A.** Schematics of the *TetO-Vegfc* transgene, *Osx-tTA-TetO-Cre* transgene, *Prox1-CreER$^{T2}$* construct, and *mT/mG* reporter. **B.** Schematic showing when *Osx-tTA;TetO-Vegfc;Prox1-CreER$^{T2}$;mT/mG* mice received doxycycline water (0.2 mg/ml) and tamoxifen (2 mg; i.p.). **C.** Representative images of serial sections stained with antibodies against Lyve1 and GFP. Femurs collected on P45 (n = 4 mice) did not contain lymphatics. The arrowheads point to Lyve1-negative-GFP-positive osteoblasts on the bone surface. Femurs collected on P65 were filled with lymphatics (n = 4 mice). The arrows point to a Lyve1-positive-GFP-positive lymphatic in bone. **D.** Approximately 85% of the Lyve1-positive lymphatics in P65 mice expressed GFP (85.98 ± 3.227, n = 4). P45 mice did not have lymphatics in bone (0 ± 0, n = 4). Data are presented as mean ± SEM. Scale bar: 50 μm.

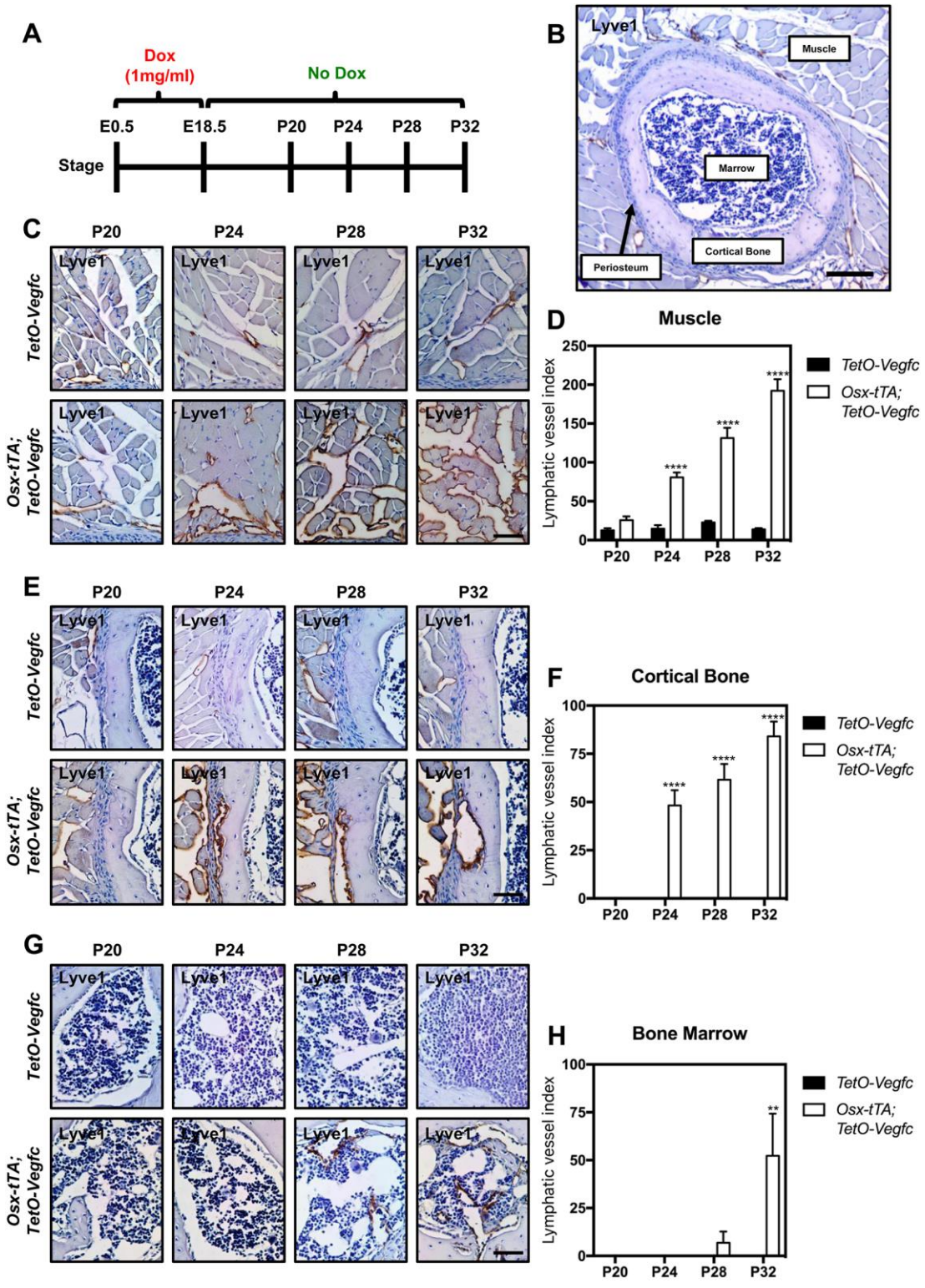


**Figure 5. Stepwise development of bone lymphatics. A.** Schematic showing when mice received doxycycline water (1 mg/ml). B. Low magnification image that shows periosseous muscle, the periosteum, cortical bone and bone marrow. These regions were imaged in *TetO-Vegfc* and *Osx-tTA-TetO-Vegfc* mice. **C.** Images of Lyve-1-positive lymphatics in intercostal muscle tissue in *TetO-*

*Vegfc* and *Osx-tTA;TetO-Vegfc* mice. **D.** Lymphatic vessel index values for muscle in P20 (12.5 ± 2.754, n=3), P24 (14.6 ± 4.581, n=5), P28 (22.8 ± 2.177, n=5), and P32 (13.79 ± 1.786, n=7) *TetO-Vegfc* mice. Lymphatic vessel index values for muscle in P20 (25.83 ± 4.604, n=3), P24 (80.8 ± 6.176, n=5), P28 (131.3 ± 13.23, n=6), and P32 (192.1 ± 14.86, n=4) *Osx-tTA;TetO-Vegfc* mice. **E.** Images of Lyve-1-positive lymphatics in cortical bone in *TetO-Vegfc* and *Osx-tTA;TetO-Vegfc* mice. **F.** Lymphatic vessel index values for cortical bone in P20 (0 ± 0, n = 3), P24 (0 ± 0, n = 5), P28 (0 ± 0, n = 5), and P32 (0 ± 0, n = 7) *TetO-Vegfc* mice. Lymphatic vessel index values for cortical bone in P20 (0 ± 0, n = 3), P24 (48.2 ± 7.96, n = 5), P28 (61.5 ± 8.172, n = 5), and P32 (84 ± 7.72, n = 4) *Osx-tTA;TetO-Vegfc* mice. **G.** Images of Lyve-1-positive lymphatics in bone marrow in *TetO-Vegfc* and *Osx-tTA;TetO-Vegfc* mice. **H.** Lymphatic vessel index values for bone marrow in P20 (0 ± 0, n = 3), P24 (0 ± 0, n = 5), P28 (0 ± 0, n = 5), and P32 (0 ± 0, n = 7) *TetO-Vegfc* mice. Lymphatic vessel index values for bone marrow in P20 (0 ± 0, n = 3), P24 (0 ± 0, n = 5), P28 (6.9 ± 5.84, n = 5), and P32 (52.25 ± 22.01, n = 4) *Osx-tTA;TetO-Vegfc* mice. Data are presented as mean ± SEM. **** $P < 0.0001$, ** $P < 0.01$; unpaired Student's *t*-test. For each timepoint, *TetO-Vegfc* mice were compared to *Osx-tTA;TetO-Vegfc* mice. Scale bars panels C, E and G: 50 μm.

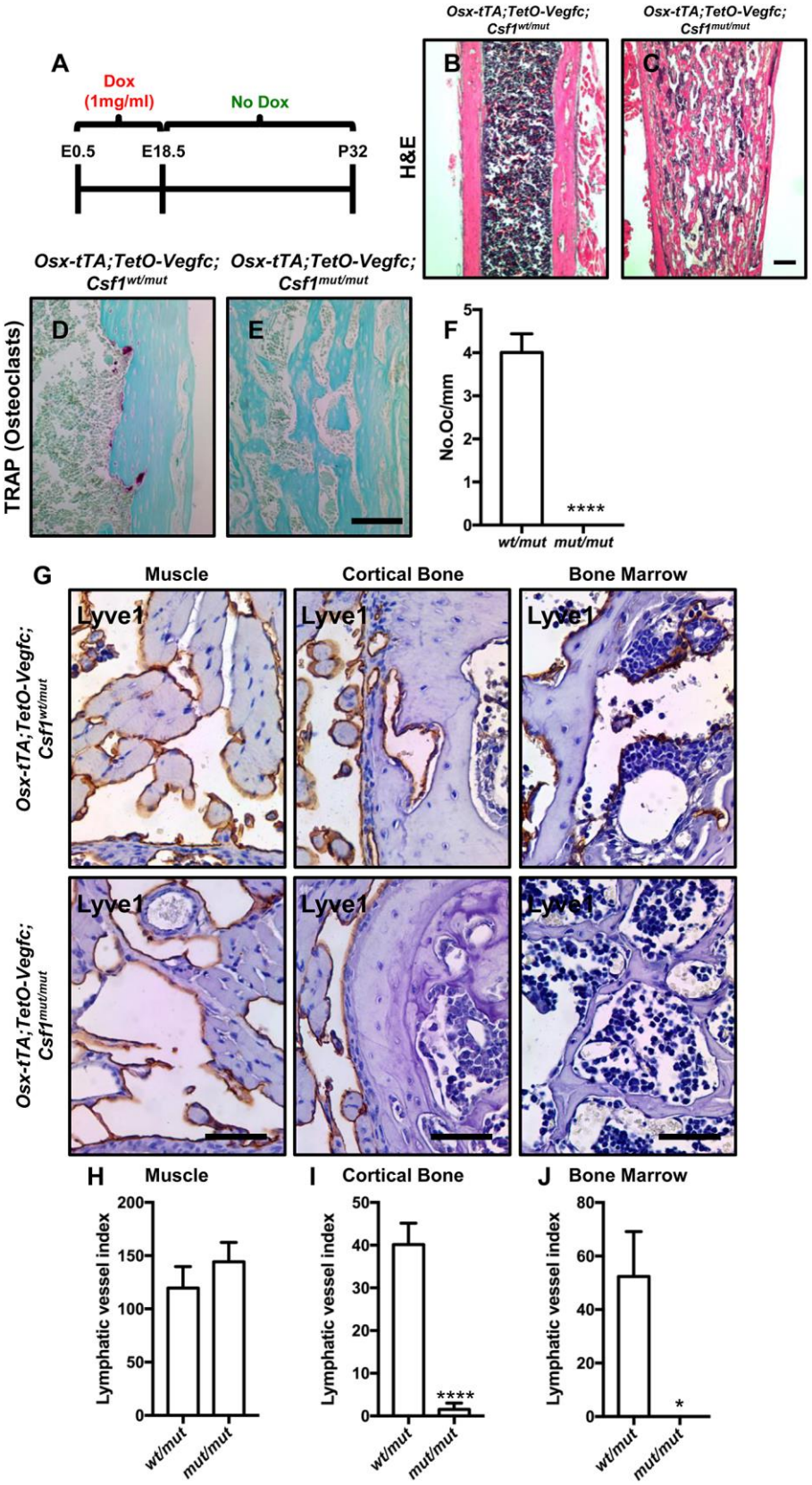


**Figure 6. The development of bone lymphatics is impaired in osteoclast-deficient mice. A.** Schematic showing when mice received doxycycline water (1 mg/ml). **B,C.** Images of H&E-stained

femur sections. *Osx-tTA;TetO-Vegfc;Csf1*$^{mut/mut}$ mice had more bone than *Osx-tTA;TetO-Vegfc;Csf1*$^{wt/mut}$ mice. Scale bar: 200 μm. **D,E.** Images of TRAP-stained femurs from *Osx-tTA;TetO-Vegfc;Csf1*$^{wt/mut}$ and *Osx-tTA;TetO-Vegfc;Csf1*$^{mut/mut}$ mice. **F.** *Osx-tTA;TetO-Vegfc;Csf1*$^{wt/mut}$ mice ($4.01 \pm 0.433$, n = 4) had significantly more osteoclasts per mm of bone surface than *Osx-tTA;TetO-Vegfc;Csf1*$^{mut/mut}$ mice ($0 \pm 0$, n = 4). **G.** Images of rib sections stained with an anti-Lyve1 antibody. **H.** The lymphatic vessel index values for muscle were not significantly different between *Osx-tTA;TetO-Vegfc;Csf1*$^{wt/mut}$ ($119.6 \pm 20.14$, n = 4) and *Osx-tTA;TetO-Vegfc;Csf1*$^{mut/mut}$ mice ($144.3 \pm 18.17$, n = 4). **I.** The lymphatic vessel index values for cortical bone were significantly different between *Osx-tTA;TetO-Vegfc;Csf1*$^{wt/mut}$ ($40.13 \pm 5.026$, n = 4) and *Osx-tTA;TetO-Vegfc;Csf1*$^{mut/mut}$ mice ($1.5 \pm 1.5$, n = 4). **J.** The lymphatic vessel index values for bone marrow were significantly different between *Osx-tTA;TetO-Vegfc;Csf1*$^{wt/mut}$ ($52.38 \pm 16.8$, n = 4) and *Osx-tTA;TetO-Vegfc;Csf1*$^{mut/mut}$ mice ($0 \pm 0$, n = 4). Data are presented as mean ± SEM. *** $P < 0.001$, * $P < 0.05$; unpaired Student's *t*-test. Scale bars: 50 μm.

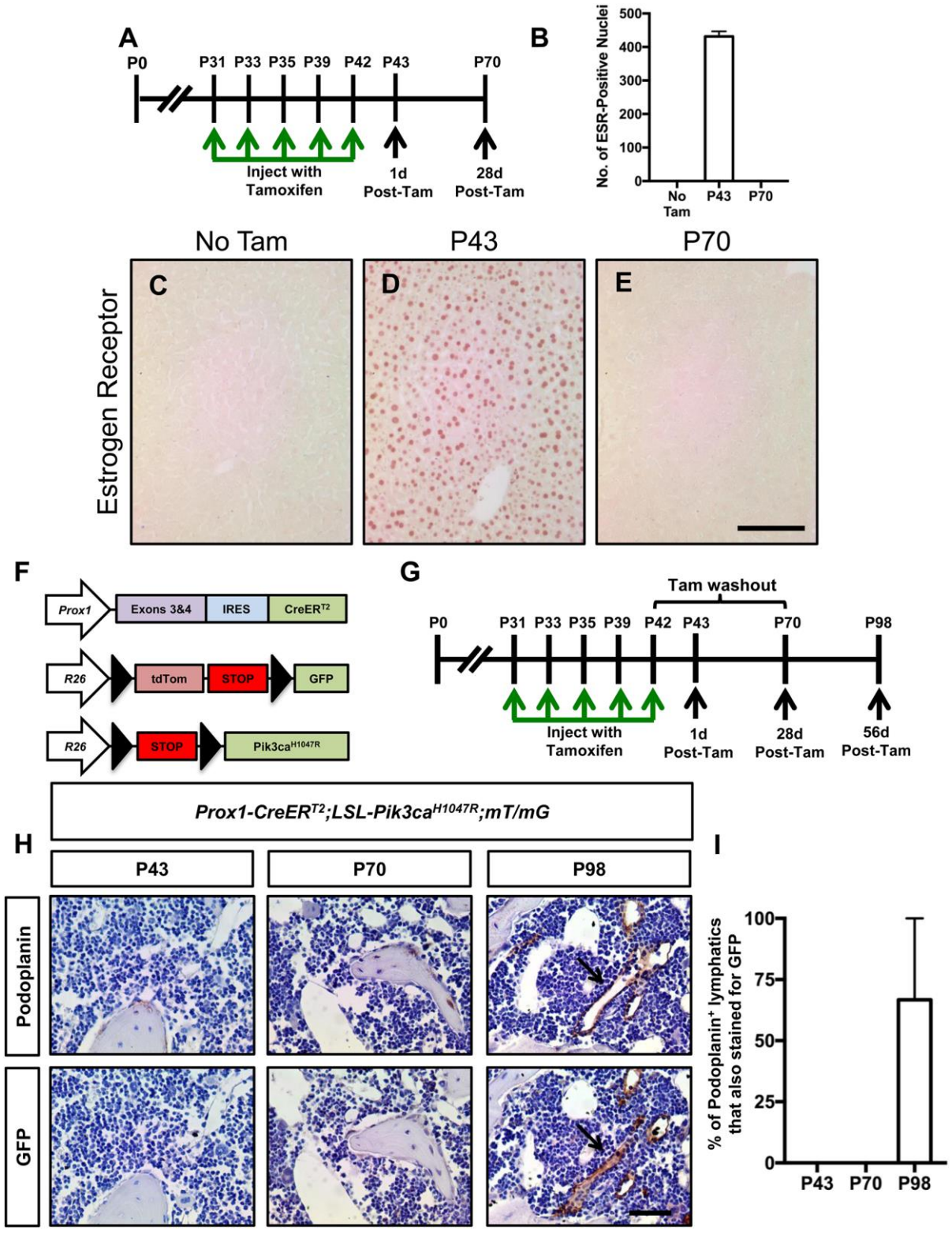


**Figure 7. Lineage tracing of Prox1-positive cells in *Prox1-CreER$^{T2}$;LSL-Pik3ca$^{H1047R}$* mice. A.** Schematic showing when *Prox1-CreER$^{T2}$* mice were injected with tamoxifen (2 mg; i.p.). **B.** Graph showing the number of estrogen receptor-positive nuclei in livers from *Prox1-CreER$^{T2}$* mice that did not receive tamoxifen (0 ± 0, n = 3), *Prox1-CreER$^{T2}$* mice 1 day after they received their last pulse of

tamoxifen (431.3 ± 15.21, n = 3), and *Prox1-CreER$^{T2}$* mice 28 days after they received their last pulse of tamoxifen (0 ± 0, n = 4). **C-E.** Representative images of livers stained with an anti-estrogen receptor antibody. CreER$^{T2}$ moved out of the nucleus within 4 weeks of mice having received their last pulse of tamoxifen. Scale bar: 100 μm. **F.** Schematics of the *Prox1-CreER$^{T2}$* allele, the *LSL-Pik3ca$^{H1047R}$* allele, and *mT/mG* reporter. **G.** Schematic showing when *Prox1-CreER$^{T2}$;LSL-Pik3ca$^{H1047R}$;mT/mG* mice were injected with tamoxifen (2 mg; i.p.). **H.** Representative images of serial sections stained with antibodies against podoplanin and GFP. Lymphatics were not present in femurs collected from *Prox1-CreER$^{T2}$;LSL-Pik3ca$^{H1047R}$;mT/mG* mice on P43 (n = 5 mice) or P70 (n = 7 mice). Lymphatics were present in 3 out of 6 mice on P98. Scale bar: 50 μm. **I.** Approximately 65% of the lymphatics in P98 bones expressed GFP (66.7 ± 33.3, n = 3). Lymphatics were not present in bones on P43 (0 ± 0, n = 5 mice) or P70 (0 ± 0, n = 7). Data are presented as mean ± SEM.

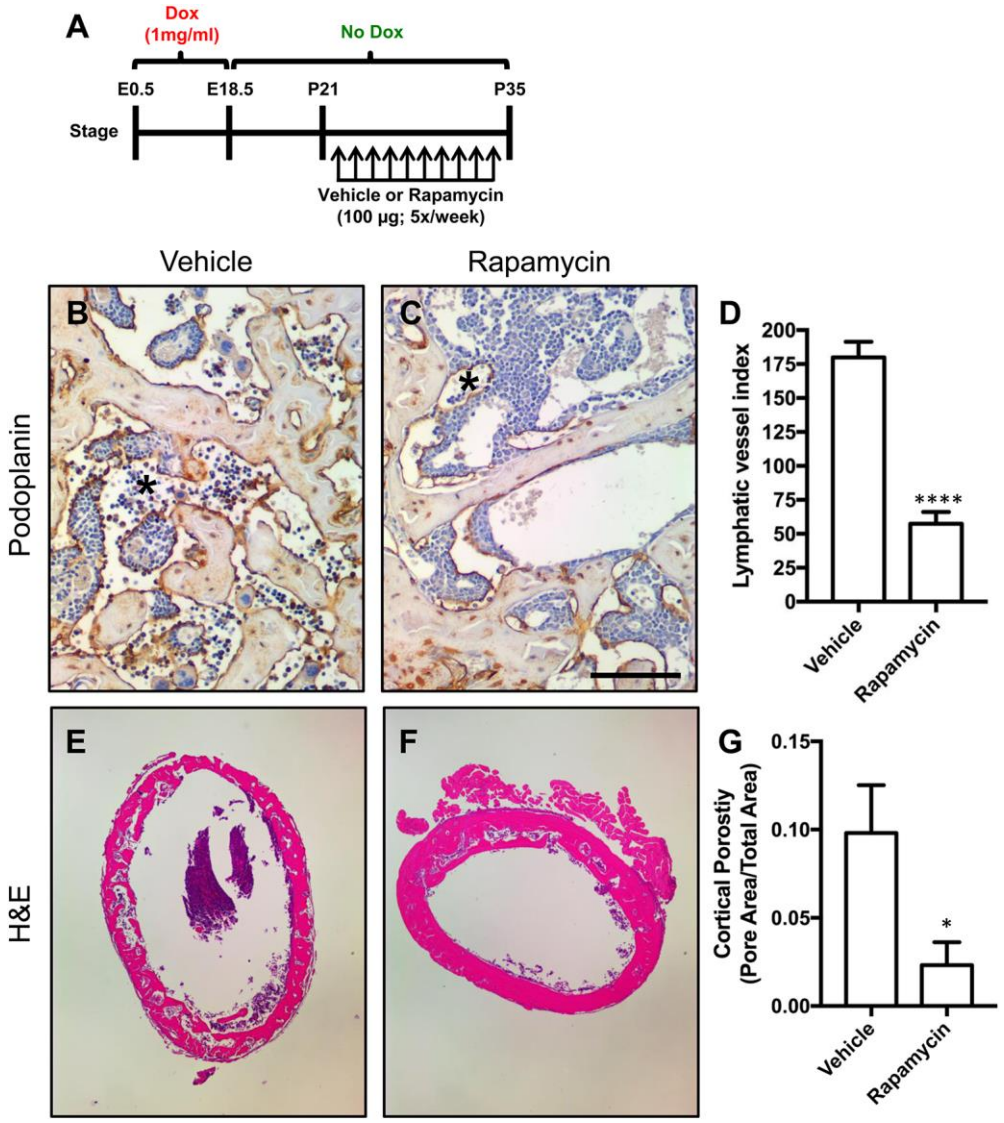


**Figure 8. Rapamycin suppresses the development of bone lymphatics in *Osx-tTA;TetO-Vegfc* mice. A.** Schematic showing when *Osx-tTA;TetO-Vegfc* mice received doxycycline water (1 mg/ml). *Osx-tTA;TetO-Vegfc* mice were treated with vehicle or rapamycin (100 µg; 5x/week; i.p.) from P21 to P35. **B,C.** Representative images of femurs stained with an anti-podoplanin antibody. The asterisks mark lymphatics containing immune cells. Bone lymphatics in *Osx-tTA;TetO-Vegfc* mice frequently contain immune cells. **D.** Lymphatic vessel index values were determined for femurs stained with an anti-podoplanin antibody. Lymphatic vessel index values were significantly higher in vehicle-treated mice (179.9 ± 11.51, n = 5) than rapamycin-treated mice (57.38 ± 8.68, n = 4). **E,F.** Representative images of femur cross sections stained with hematoxylin and eosin. **G.** Cortical porosity values for vehicle (0.098 ± 0.027, n = 4) and rapamycin-treated mice (0.023 ± 0.013, n = 5). Data are presented as mean ± SEM. * $P < 0.05$; **** $P < 0.0001$; unpaired Student's *t*-test. Scale bar: 100 µm.

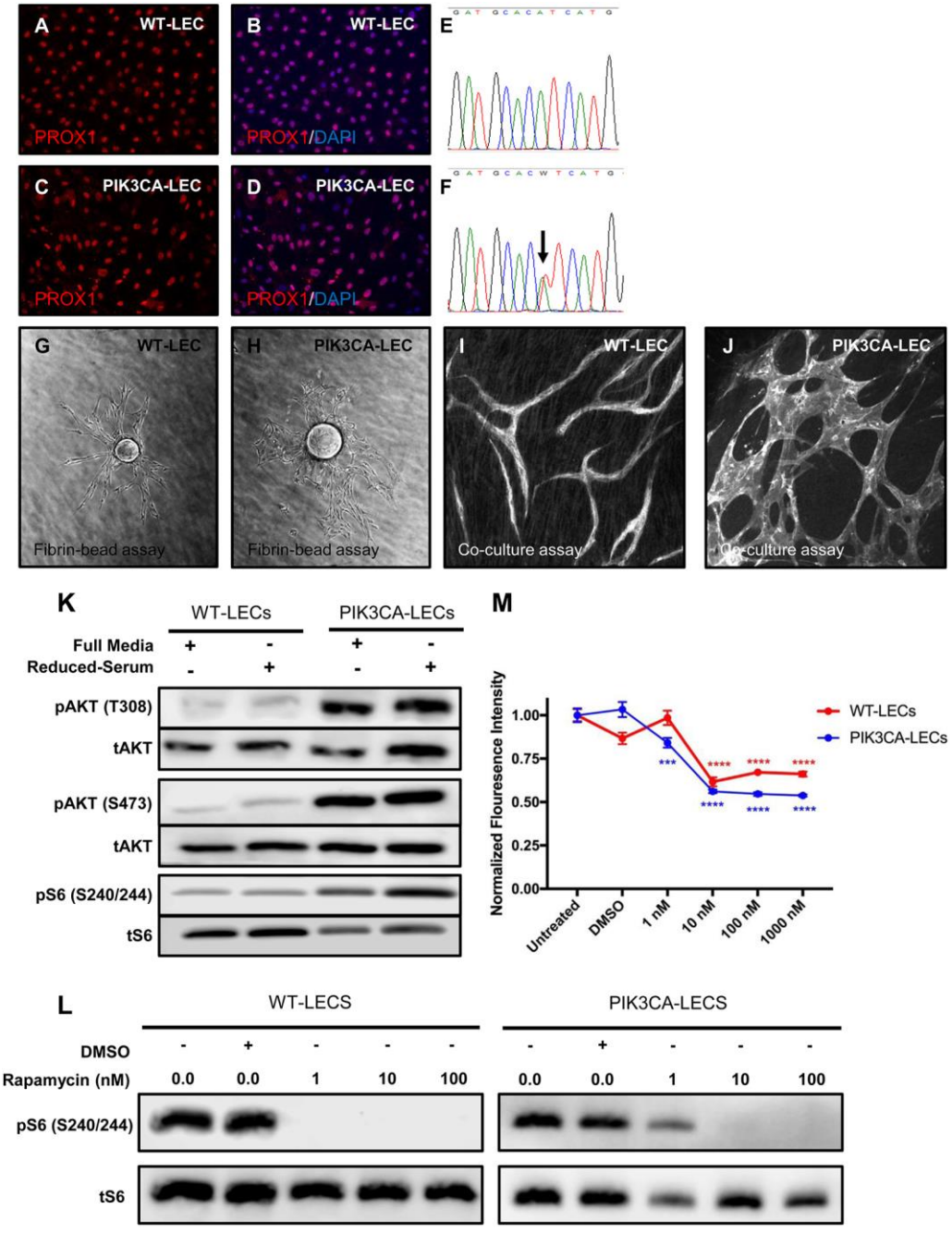


**Figure 9. PIK3CA-LECs form irregular vessels *in vitro* and rapamycin suppresses the growth of PIK3CA-LECs. A-D.** PROX1 immunostaining results for WT-LECs and PIK3CA-LECs. **E,F.** Sanger sequencing results for WT-LECs and PIK3CA-LECs. PIK3CA-LECs have a somatic activating mutation in *PIK3CA* (arrow). **G,H.** Fibrin-bead assay results for WT-LECs and PIK3CA-LECs. PIK3CA-LECs formed hyperplastic vessels. **I,J.** Fibroblast co-culture assay results for WT-LECs and PIK3CA-LECs. PIK3CA-LECs formed hyperplastic vessels. **K.** Immunoblot analysis with lysates from WT-LECs and PIK3CA-LECs. Lysates were made of cells cultured in full growth media or of cells cultured overnight in reduced-serum media. The levels of pAKT and pS6 were greater in

PIK3CA-LECs than WT-LECs. **L.** Immunoblot analysis with lysates from cells treated with DMSO (vehicle) or rapamycin. Cells were treated with drug for 24 hours. Rapamycin blocked mTORC1 signaling in WT-LECs and PIK3CA-LECs. **M.** WT-LECs and PIK3CA-LECs were treated with DMSO or rapamycin (1, 10, 100, or 1000 nM) for 3 days. Cell viability was measured with a Cell-Titer Blue kit. Statistical significance was measured by ANOVA followed by a Dunnett's multiple comparisons test. Groups were compared to the untreated group. Data are presented as mean ± SEM. *** $P < 0.001$; **** $P < 0.0001$

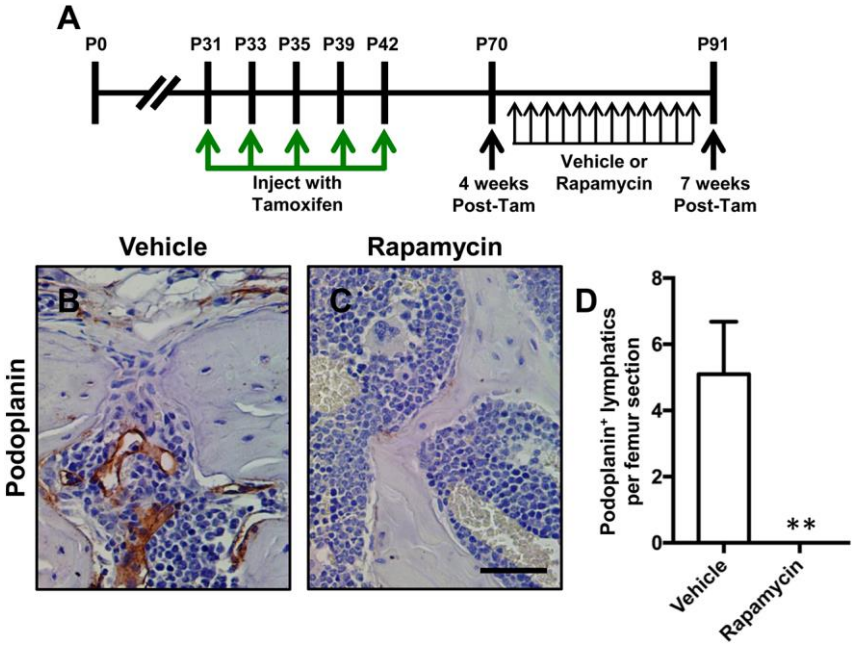


**Figure 10. Rapamycin suppresses the development of bone lymphatics in *Prox1-CreER$^{T2}$;LSL-Pik3ca$^{H1047R}$* mice. A.** Schematic showing when *Prox1-CreER$^{T2}$;LSL-Pik3ca$^{H1047R}$* mice were injected with tamoxifen (2 mg; i.p.). *Prox1-CreER$^{T2}$;LSL-Pik3ca$^{H1047R}$* mice were treated with vehicle or rapamycin (100 μg; 5x/week; i.p.) from P70 to P91. **B,C.** Representative images of femurs stained with an anti-podoplanin antibody. **D.** Femurs from vehicle-treated mice (5.1 ± 1.581, n=10) had significantly more lymphatics than femurs from rapamycin-treated mice (0 ± 0, n=10). Data are presented as mean ± SEM. ** $P < 0.01$; unpaired Student's *t*-test. Scale bar: 50 μm.

**Table 1. Description of the mouse strains in this study.**

| Strain | Description | Reference |
|---|---|---|
| *Csf1*$^{mut}$ | Mice have a signle base pair insertion in *Csf1* that results in the formation of a truncated protein. Homozygous mutant mice have a defect in the development of macrophages and osteoclasts. | Yoshida et al., 1990. |
| *LSL-Pik3ca*$^{H1047R}$ | The strain carries a floxed transcriptional stop cassette upstream of an active form of *Pik3ca* in the *Rosa26* locus. | Adams et al., 2011. |
| *Lyve1-Cre* | The *Lyve1-Cre* allele labels lymphatic endothleial cells, macrophages, a subset of hematopoietic stem cells, and blood vessels in the lung, liver and yolk sac. | Pham et al., 2010. |
| *mT/mG* | This strain has a Cre-inducible GFP reporter at the *Rosa26* locus. | Muzumdar et al., 2007. |
| *Prox1-CreER*$^{T2}$ | These mice express a CreER$^{T2}$ fusion protein from the endogenous *Prox1* locus. CreERT2 activity is present in lymphatic endothelial cells, cardiomyocytes, hepatocytes, pancreatic ducts, islets, and neurons. | Rodriguez-Laguna et al., 2019. Srinivasan et al., 2007. |
| *Osx-tTA-TetO-Cre* | Transgenic mice that express a tetracycline transactivator protein and Cre recombinase in osteoblasts, osteocytes and chondrocytes. This is a Tet-Off strain. | Rodda and McMahon, 2006. |
| *TetO-Vegfc* | The expression of VEGFC can be controlled by doxycycline when bred with wither a tTA (Tet-Off) or rtTA (Tet-On) driver. | Lohela et al., 2008. |

**Table 2. Lymphatic vessel index values for *TetO-Vegfc* and *Osx-tTA;TetO-Vegfc* mice.**

| | Muscle | | Cortical Bone | | Bone Marrow | |
|---|---|---|---|---|---|---|
| **Age** | ***TetO-Vegfc*** | ***Osx-tTA-TetO-Vegfc*** | ***TetO-Vegfc*** | ***Osx-tTA-TetO-Vegfc*** | ***TetO-Vegfc*** | ***Osx-tTA-TetO-Vegfc*** |
| P20 | 12.5 ± 2.754, n=3 | 25.83 ± 4.604, n=3 | 0 ± 0, n = 3 | 0 ± 0, n = 3 | 0 ± 0, n = 3 | 0 ± 0, n = 3 |
| P24 | 14.6 ± 4.581, n=5 | 80.8 ± 6.176, n=5**** | 0 ± 0, n = 5 | 48.2 ± 7.96, n = 5**** | 0 ± 0, n = 5 | 0 ± 0, n = 5 |
| P28 | 22.8 ± 2.177, n=5 | 131.3 ± 13.23, n=6**** | 0 ± 0, n = 5 | 61.5 ± 8.172, n = 5**** | 0 ± 0, n = 5 | 6.9 ± 5.84, n = 5 |
| P32 | 13.79 ± 1.786, n=7 | 192.1 ± 14.86, n=4**** | 0 ± 0, n = 7 | 84 ± 7.72, n = 4**** | 0 ± 0, n = 7 | 52.25 ± 22.01, n = 4** |

**** $P < 0.0001$, ** $P < 0.01$

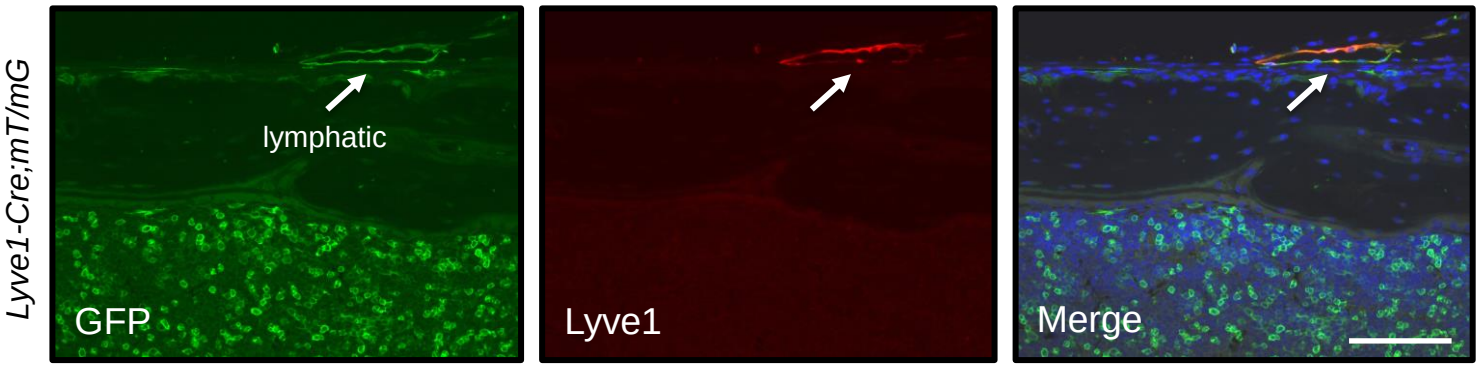


**Fig S1. Cells labeled by *Lyve1-Cre* do not express Lyve1.** Femurs from *Lyve1-Cre;mT/mG* were stained with antibodies against GFP (green) and Lyve1 (red) and counterstained with DAPI (blue). The GFP positive cells in the marrow cavity do not express Lyve1. However, the lymphatic in the periosseous connective tissue (arrow) expresses GFP and Lyve1. Scale bar: 100 μm.

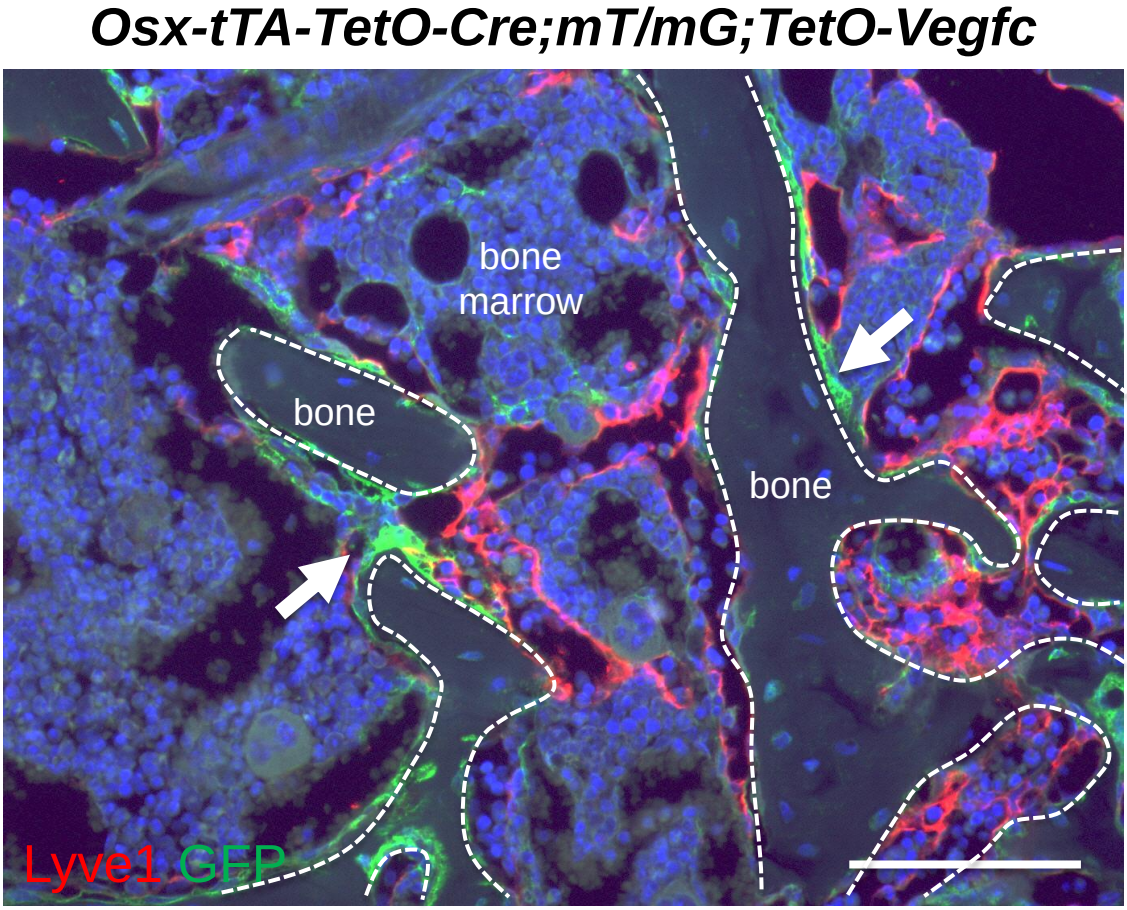


**Fig S2. Bone cells in *Osx-tTA-TetO-Cre;TetO-Vegfc;mT/mG* mice express GFP.** The arrows point to GFP-positive cells on the surface of bone in an *Osx-tTA-TetO-Cre;TetO-Vegfc;mT/mG* mouse. The Lyve1-positive lymphatics do not express GFP. Scale bar: 100 μm.

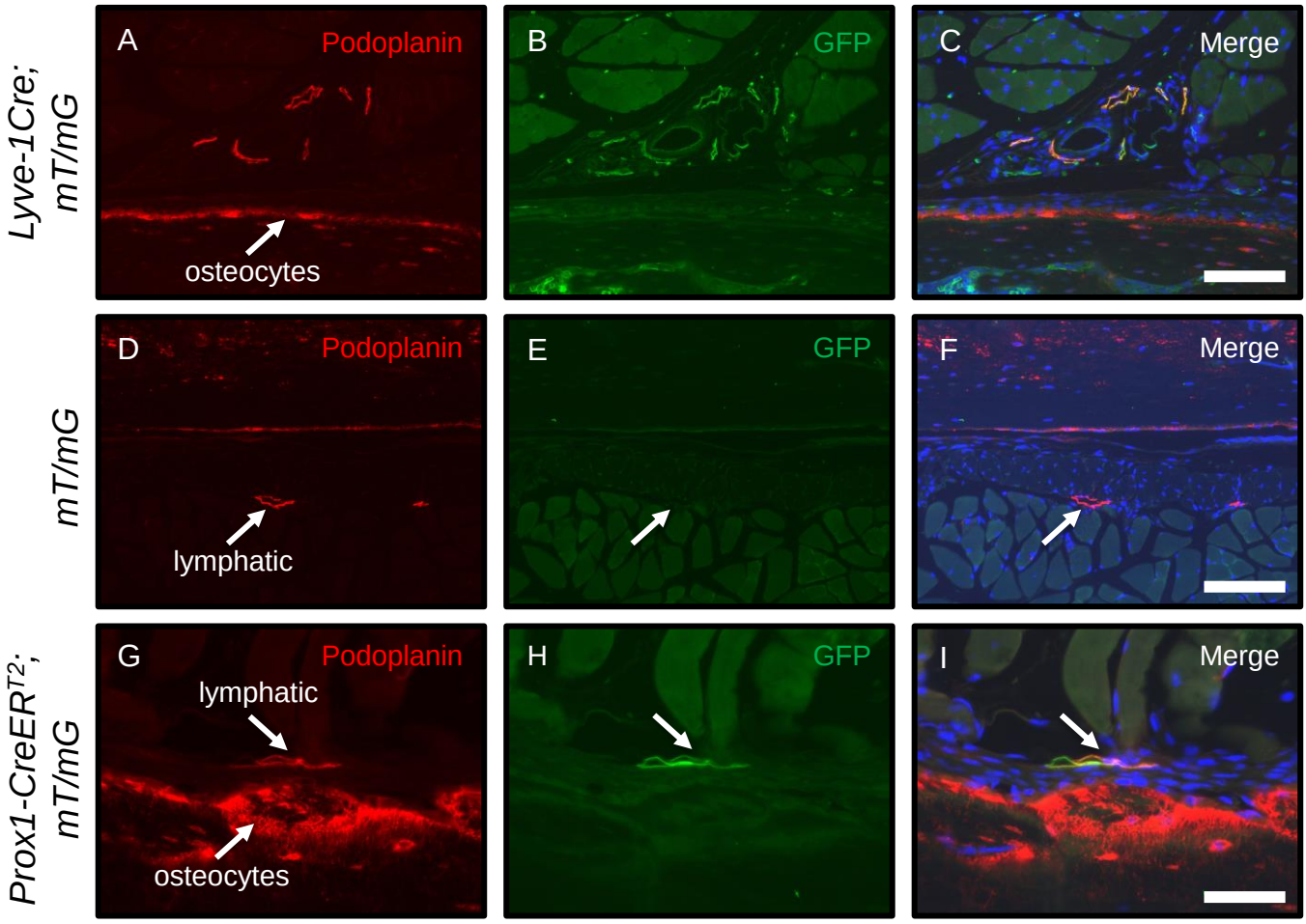


**Fig S3. Periosseous lymphatics in *Prox1-CreER$^{T2}$;mT/mG* mice express GFP.** Femurs from *Lyve1-Cre;mT/mG* mice (positive control for immunostaining for GFP; A-C; n = 3 mice), *mT/mG* mice (negative control for immunostaining for GFP; D-F; n = 3 mice) and *Prox1-CreER$^{T2}$;mT/mG* mice (G-I; n = 3 mice) were stained with antibodies against podoplanin and GFP. Periosseous lymphatics and osteocytes expressed podoplanin. Periosseous lymphatics in *Lyve1-Cre;mT/mG* mice and *Prox1-CreER$^{T2}$;mT/mG* mice expressed GFP. Scale bar in panels C and F: 100 μm. Scale bar in panel I: 50 μm.

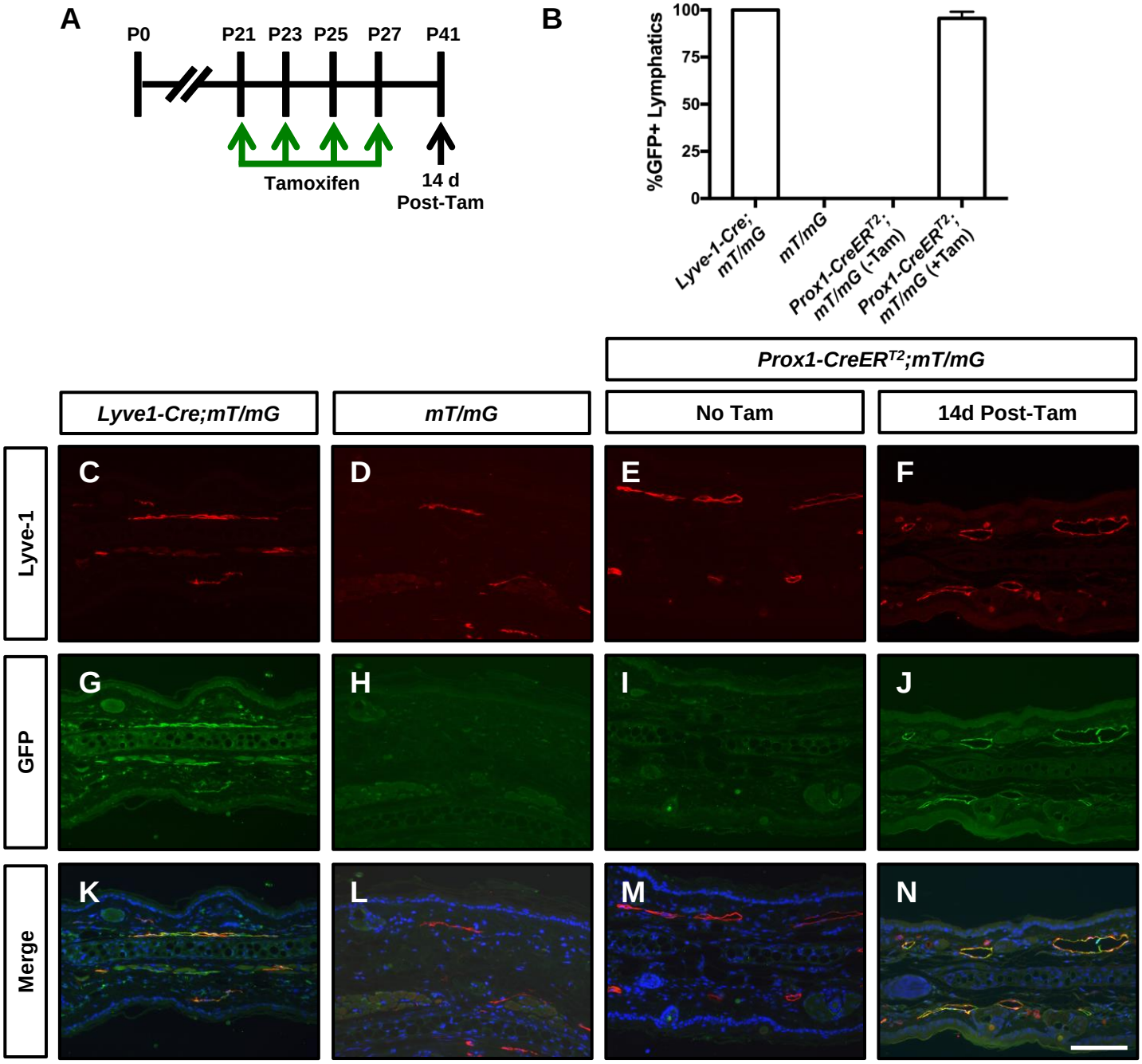


**Fig S4. The *Prox1-CreER$^{T2}$* allele is not active in the absence of tamoxifen. A.** Schematic showing when *Prox1-CreER$^{T2}$;mT/mG* mice were injected with tamoxifen (2 mg; i.p.). **B.** Graph showing the percent of GFP-positive lymphatics in the skin of *Lyve-1Cre;mT/mG* mice (100 ± 0, n = 3), *mT/mG* mice (0 ± 0, n = 2), *Prox1-CreER$^{T2}$;mT/mG* mice that did not receive tamoxifen (0 ± 0, n = 3), and *Prox1-CreER$^{T2}$;mT/mG* mice that received tamoxifen (95.6 ± 3.4, n = 3). **C-N**. Representative images of ear skin sections stained with antibodies against Lyve-1 and GFP. Data are presented as mean ± SEM. Scale bar: 100 μm.

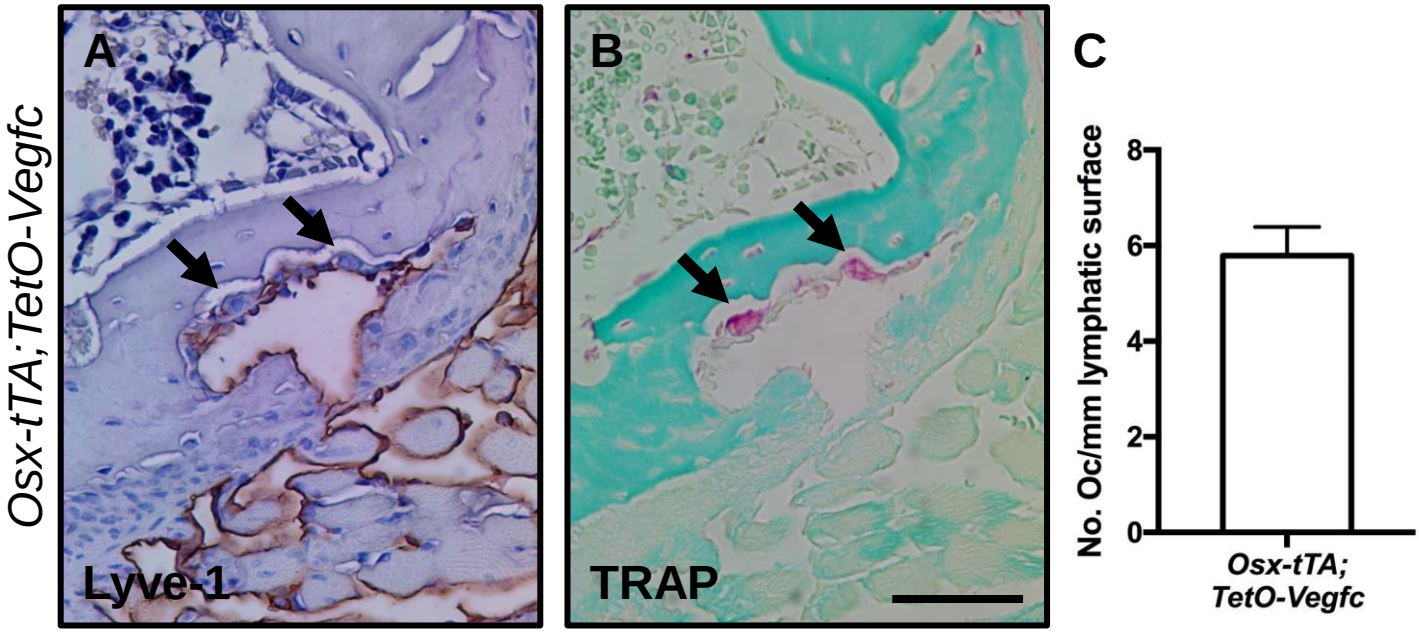


**Fig S5. Osteoclasts are closely associated with lymphatics invading bone in *Osx-tTA;TetO-Vegfc* mice.** **A,B.** Representative images of rib serial sections stained for Lyve1 (A) and TRAP activity (B). The arrows in panels A and B point to osteoclasts. **C.** Graph showing the number of osteoclasts per millimeter of lymphatic surface ($5.8 \pm 0.61$; $n = 3$). Scale bar: 50 μm.